

OPEN ACCESS

EDITED BY
Katrina Traber,
Boston University, United States

REVIEWED BY Bikash Sahay, University of Florida, United States Rong Mou, Guizhou Medical University, China

*CORRESPONDENCE
Adrianus C. M. Boon
jboon@wustl.edu
Makedonka Mitreva
mmitreva@wustl.edu

[†]These authors have contributed equally to this work and share first authorship

[†]These authors have contributed equally to this work and share last authorship

RECEIVED 09 September 2025 ACCEPTED 22 October 2025 PUBLISHED 05 November 2025

CITATION

Rosa BA, Bigham M, Darling TL, Arun A, Singh KS, Martin J, Boon ACM and Mitreva M (2025) Hookworm infection modulates lung and intestinal transcriptomic responses to SARS-CoV-2 in Syrian hamsters. *Front. Immunol.* 16:1701728. doi: 10.3389/fimmu.2025.1701728

COPYRIGHT

© 2025 Rosa, Bigham, Darling, Arun, Singh, Martin, Boon and Mitreva. This is an openaccess article distributed under the terms of the Creative Commons Attribution License (CC BY). The use, distribution or reproduction in other forums is permitted, provided the original author(s) and the copyright owner(s) are credited and that the original publication in this journal is cited, in accordance with accepted academic practice. No use, distribution or reproduction is permitted which does not comply with these terms.

Hookworm infection modulates lung and intestinal transcriptomic responses to SARS-CoV-2 in Syrian hamsters

Bruce A. Rosa^{1†}, Mahdiyeh Bigham^{1†}, Tamarand L. Darling^{1†}, Ashutosh Arun¹, Kumar Sachin Singh¹, John Martin¹, Adrianus C. M. Boon^{1,2,3*‡} and Makedonka Mitreva^{1,4,5*‡}

¹Division of Infectious Diseases, Department of Medicine, Washington University School of Medicine, St. Louis, MO, United States, ²Department of Molecular Microbiology, Washington University School of Medicine, St. Louis, MO, United States, ³Department of Pathology and Immunology, Washington University School of Medicine, St. Louis, MO, United States, ⁴Department of Genetics, Washington University School of Medicine, St. Louis, MO, United States, ⁵McDonnell Genome Institute, Washington University School of Medicine, St. Louis, MO, United States

Background: Helminth infections are widespread in resource-limited settings, and modulate host immune responses, with potential implications for viral coinfections. Intestinal helminths can alter susceptibility to respiratory viruses, but the mechanisms influencing SARS-CoV-2 infection outcomes remain poorly understood.

Methods: Using the Syrian hamster model, we investigated the impact of prior infection with the human hookworm *Ancylostoma ceylanicum* on host responses to SARS-CoV-2. Tissue-specific transcriptional responses were compared among four groups: naive, hookworm-only, SARS-CoV-2-only, and coinfected with both pathogens, 3 and 6 days post-viral infection. Viral titers and weight loss were assessed, and RNA-seq transcriptome profiles from lung and intestinal tissues were interrogated to identify differentially expressed genes and cellular pathways.

Results: Prior hookworm infection did not significantly alter viral titers or weight loss compared to SARS-CoV-2 infection alone, but distinct transcriptional signatures compared were identified compared to either single infection. Coinfection uniquely differentially regulated hematopoiesis and B cellassociated genes (e.g., ATF5, IGHM, JCHAIN) in the lungs, and immune and stress response pathways and inflammation-associated genes (e.g. FOLR2, PLA2GF, FABP3) in the intestine. Genes and pathways differentially regulated by SARS-CoV-2 alone, but with attenuated transcriptional responses in the lungs of coinfected hamsters were observed, including the loss of upregulation of toll-like receptor signaling and previously proposed host biomarkers for COVID-19 severity (CHI3L1, HMOX1), Long COVID (FCG4/FCGR3A and FST) and mortality (FST). In the intestine, hookworm-associated suppression of type I interferonrelated genes (TAP1, IRF7) was reversed with SARS-CoV-2 coinfection, highlighting pathogen-specific modulation of innate antiviral signaling. Genes and pathways consistently differentially regulated by with SARS-CoV-2 were consistent with expectations, and many hemoglobin pathways were differentially regulated with hookworm in the intestine. CIBERSORT analysis was estimated relative leukocyte abundances in each sample cohort.

Conclusion: Our findings demonstrate that *A. ceylanicum* infection reshapes host transcriptional responses to SARS-CoV-2 in a tissue-specific manner, enhancing B cell immunity in the lung while driving intestinal inflammation. Hookworm-induced immune modulation attenuated key SARS-CoV-2-responsive genes and pathways, suggesting potential mechanisms for reduced disease severity observed in helminth-endemic regions. These findings establish a molecular framework to better understand helminth, SARS-CoV-2 and host immune interactions, with relevance for other respiratory viral infections.

KEYWORDS

hookworm, SARS-CoV-2, coinfection, host response, transcriptomics, helminth-virus interaction, immune modulation

1 Introduction

The SARS-CoV-2 pandemic presented a significant global health challenge, resulting in 777 million total reported infection cases and more than 7 million deaths reported worldwide (1, 2). Individuals aged 65 and older remain at risk for infection, as they are severely affected by severe COVID-19, accounting for 80% of hospitalizations and exhibiting a 23-fold increase in mortality compared to younger age groups. Age-associated alterations likely influence this increased susceptibility in immune system efficiency, genetic regulation, cellular metabolism, and inflammatory processes (3). Contrary to early predictions of severe outcomes in Africa, the continent has recorded comparatively lower infection and mortality rates from the start of the pandemic in 2020 to 2022-2023. While the median age in Africa is lower compared to other continents, coinfections with other pathogens may have reduced the impact of the COVID-19 pandemic. Emerging evidence suggests that coinfection with malaria can alter disease outcomes, potentially improving survival rates in some cases (4). This interaction highlights the complex immune modulation induced by chronic malaria parasite exposure, which may influence the progression of viral infections. Understanding these coinfection dynamics could provide new insights for disease management and therapeutic strategies in regions burdened by both malaria and viral epidemics. Specifically, hookworm infections affect approximately 472 million people in resource-limited rural areas, resulting in over 4 million disability-adjusted life years (DALYs) lost annually and imposing an economic burden exceeding US\$100 billion per year (5).

Chronic and acute hookworm infections can modulate the host immune system by inducing a type 2 (Th2) immune response and overall immune functionality (6). Helminths modify the immune

Abbreviations: CoV, Cohort of hamsters infected only with SARS-CoV-2; HW, Cohort of hamsters infected only with hookworm (*A. ceylanicum*); HW+CoV, Cohort of hamsters infected with hookworm followed by SARS-CoV-2; DEGs, Differentially expressed genes (significant according to DESeq2 analysis); GO, Gene Ontology; KEGG, Kyoto Encyclopedia of Genes and Genomes.

system by secretion of immunomodulatory molecules that regulate host innate and adaptive immune responses (7, 8). These changes can significantly impact disease progression and clinical presentation during coinfection with other pathogens including respiratory viruses. Before 2019, helminth infections were demonstrated to confer protection against the influenza and respiratory syncytial virus (RSV) in mouse disease models. This protective effect was linked to the activation of effector CD4⁺ and CD8⁺ T cells (9), which enhance immune responses by upregulating type I interferons, pro-inflammatory cytokines, and antiviral factors such as interferon stimulated genes (*ISG*), and *CRAMP* gene expression in the lungs and duodenum (10). It was shown that coinfection of mice with the helminths *Trichinella* spiralis or *Heligmosomoides polygyrus* and influenza virus alters immune responses and lung pathology (11).

In a study of 751 SARS-CoV-2 patients in Africa, infection with intestinal helminths was associated with a significantly lower probability of developing severe COVID-19 (12), and chronic helminth infections are thought to suppress SARS-CoV-2 entry and hyperinflammation, by attenuating inflammatory signaling pathways and suppressing the release of pro-inflammatory cytokines (13). Additionally, helminth extracts applied *in vitro* to PBMCs isolated from SARS-CoV-2 patients modulate immune reactivity to SARS-CoV-2 peptides by suppressing reactive CD4+ helper T cells but maintaining reactive CD8+ cytotoxic T cells (14).

Animal models to study helminth and SARS-CoV-2 coinfection present an opportunity to better understand these mechanisms using different helminth species. Previous research in hamsters has investigated specific aspects of COVID-19 coinfection with parasitic helminths, such as *Schistosoma* (15), and assessed the impacts of the COVID-19 pandemic on neglected tropical diseases (NTDs) (16). In mice, prior infection with the lung-migrating rodent helminth *Nippostrongylus brasiliensis* enhances the immune system's response to SARS-CoV-2, improving viral clearance and reducing disease severity by boosting CD8+ T cell recruitment and activation, a process that depends on macrophages in mice (17). In another mouse study, infection with the pork tapeworm *T. spiralis* indicated

that anti-inflammatory markers from its secreted products may mitigate adverse pathology from SARS-CoV-2 infection (18). While informative, mice are not natural hosts for these viruses or helminths, and laboratory mice are pathogen-free, which has a significant impact on disease induced by viruses (19, 20) and potentially worms (11, 19, 21).

In this study, we aimed to investigate the impact of experimental infection with the human-parasitic intestinal hookworm *Ancylostoma ceylanicum* using a Syrian hamster SARS-CoV-2 model. This experimental model represents the first helminth-SARS-CoV-2 study to examine whole-transcriptome profiling of host responses, facilitating the discovery of novel genes and pathways involved beyond targeted immune profiling performed in previous studies. We utilized separate single-infection and coinfection cohorts to analyze the transcriptome responses of both the lung and the intestine (at 3 days and 6 days post-SARS-CoV-2 infection), to comprehensively characterize the distinct host responses associated uniquely with coinfection in a tissue-specific manner. The results identify known and published differentially expressed genes, as well as many novel responsive genes and pathways of interest for future studies.

2 Materials and methods

2.1 Ethics statements

All animal experiments were carried out under protocols approved by Washington University School of Medicine Institutional Animal Care and Use Committees (assurance number A3381-01). All housing and care of laboratory animals conformed to the National Institutes of Health (NIH) Guide for the Care and Use of Laboratory Animals in Research (see 18-F22) and all requirements and regulations issued by the United States Department of Agriculture (USDA), including regulations implementing the Animal Welfare Act (P.L. 89-544) as amended (see 18-F23).

2.2 Cells and viruses

Vero cells expressing human angiotensin converting enzyme 2 (ACE2) and transmembrane protease serine 2 (TMPRSS2) (Vero-hACE2-hTMPRSS2, gift of Adrian Creanga and Barney Graham, NIH) were cultured at 37 °C in Dulbecco's Modified Eagle medium (DMEM) supplemented with 10% fetal bovine serum (FBS), 10 mM HEPES (pH 7.3), 2 mM L-glutamine, 100 U/mL Penicillin, 100 µg/mL Streptomycin, and 10 µg/mL of puromycin. Vero E6 cells expressing human TMPRSS2 (Vero-hTRMPRSS2) were cultured at 37 °C in DMEM supplemented with 10% FBS, 10 mM HEPES (pH 7.3), 2 mM L-glutamine, 100 U/mL Penicillin, 100 µg/mL Streptomycin, and 5 µg/mL of blasticidin. Vero-hACE2-hTRMPSS2 are used to titrate stocks and tissues and Vero-hTRMPSS2 cells are used to generate virus stocks. SARS-CoV-2 (strain 2019-nCoV/USA-WA1/2020) was obtained from the US

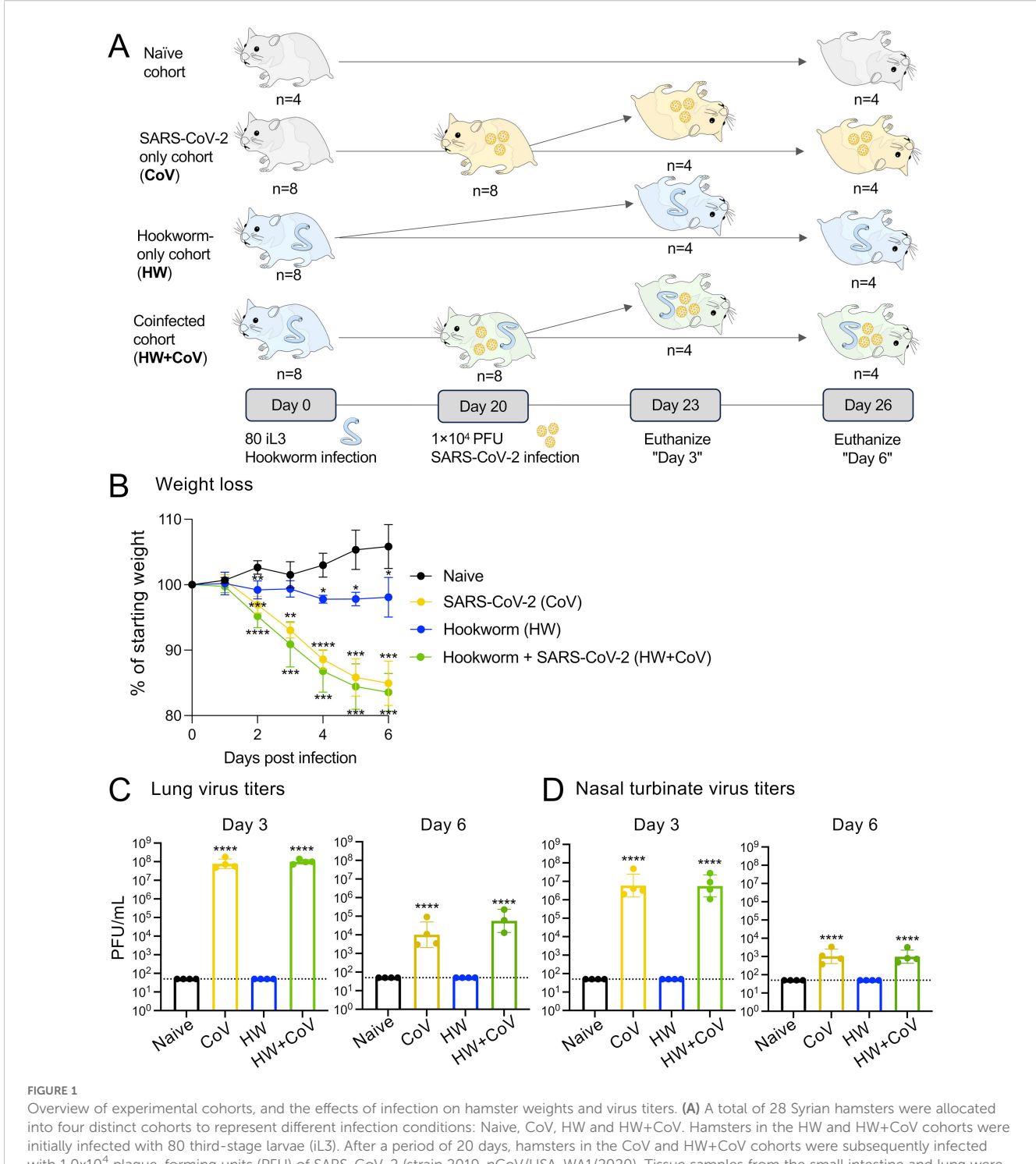
Centers for Disease Control (CDC) and the virus stock sequence was confirmed by next-generation sequencing prior to *in vitro* or *in vivo* use. All work with infectious SARS-CoV-2 was performed in Institutional Biosafety Committee approved BSL-3 and ABSL3 facilities at Washington University School of Medicine using appropriate positive pressure air respirators and protective equipment.

2.3 Hamster infection and euthanasia

Twenty-eight male hamsters, aged five to six weeks old, were purchased from Charles River Laboratory and split into four cohorts to represent uninfected (naive), hookworm-only (HW), virus-only (CoV), and worm-virus coinfected (HW+CoV) cohorts. The HW and HW+CoV cohorts were inoculated by oral gavage with 80 infected L3 (iL3) at day 0. Twenty days post hookworm infection, both the CoV and HW+CoV cohorts were intranasally inoculated with 1.0×10⁴ PFU SARS-CoV-2 (strain 2019-nCoV/ USA-WA1/2020) in 100 µL following isoflurane sedation. Weights were recorded daily for all cohorts after viral inoculation. At day 23 and 26, hamsters were euthanized using appropriate technique, equipment, and agents. Compressed CO2 gas in cylinders were used as a source of carbon dioxide, allowing for the controlled inflow of gas to the induction chamber. Hamsters to be euthanized were placed in a clean transparent chamber and 100% CO₂ was introduced at a fill rate of 70% of the chamber volume per minute, to achieve a balanced gas mixture with the existing air in the chamber to fulfill the objective of rapid unconsciousness with minimal distress to the animals. Expected time to unconsciousness was usually within 3-5 minutes. Each hamster was monitored for lack of respiration and faded eye color. CO2 was maintained for a minimum of 1 minute after observing these signs to avoid unintended recovery upon exposure to natural CO2 concentrations. Upon completion of the procedure, death was confirmed by ascertaining cardiac and respiratory arrest and noting an animal's fixed and dilated pupils. Organs were dissected as described below and collected for infectious titer and RNA-seq analysis. All sample cohorts, including the control, include four biological replicates. A detailed sample collection timeline is provided in Figure 1A.

2.4 Infectious viral titer

At time of collection, the right lung lobe and nasal turbinate were collected. Nasal turbinates were collected by removing the skin along the nose and cheeks then cutting the jaw to expose the upper palate. A sagittal incision through the palate exposed the nasal turbinates, which were then removed using blunt forceps. The right lung and nasal turbinates were homogenized in 1.0 mL DMEM and clarified by centrifugation at 1,000×g for five minutes. Plaque assays were performed on Vero-hACE2-hTRMPSS2 cells in 24-well plates. Lung tissue homogenates and nasal turbinate homogenates were serially diluted in cell infection medium (DMEM supplemented



Overview of experimental cohorts, and the effects of infection on hamster weights and virus titers. (A) A total of 28 Syrian hamsters were allocated into four distinct cohorts to represent different infection conditions: Naive, CoV, HW and HW+CoV. Hamsters in the HW and HW+CoV cohorts were initially infected with 80 third-stage larvae (iL3). After a period of 20 days, hamsters in the CoV and HW+CoV cohorts were subsequently infected with 1.0×10^4 plaque-forming units (PFU) of SARS-CoV-2 (strain 2019-nCoV/USA-WA1/2020). Tissue samples from the small intestine and lung were collected at two time points: 3 days (day 23) and 6 days (day 26) after the CoV infection timepoint (referred to as day 3 and day 6 for the analysis). (B) Hamster body weight for each of the three infection cohorts (CoV, HW and HW+CoV) was compared to the naive cohort at each day of infection using a two-way ANOVA mixed-effects model with Dunnett's multiple comparison testing. After hamsters were sacrificed (at day 3 and day 6), SARS-CoV-2 virus titers were measured in (C) lung tissue and (D) nasal turbinates, compared to the naive cohort using a one-way ANOVA with Dunnett's multiple comparison test. Error bars represent standard deviation values; $*P \le 0.05$, $**P \le 0.01$, $***P \le 10^{-3}$, $*****P \le 10^{-4}$.

with 2% FBS, 10 mM HEPES [pH 7.3] and 2 mM L-glutamine). Two hundred microliters of the diluted virus were added to a single well per dilution per sample. After one hour at 37 °C, the inoculum was aspirated, the cells were washed with PBS, and a 1%

methylcellulose overlay in MEM supplemented with 2% FBS was added. Seventy-two hours after virus inoculation, the cells were fixed with 10% formalin, and the monolayer was stained with crystal violet (0.5% w/v in 25% methanol in water) for one hour

at 20 °C. The number of plaques were counted and used to calculate the plaque forming units/mL (PFU/mL). Infectious virus titer detected in any of the contact hamster organs was considered a positive transmission event.

2.5 RNA preparation and sequencing

At time of collection, the remaining lung lobes and a dissection of the small intestine were collected for RNA-seq analysis. A 4 cm piece of the anterior end of the small intestine (near the duodenum, 1-1.5 cm after the stomach) was cut and opened longitudinally. The contents were washed out with PBS three times, and the piece was split into two 2 cm halves. One half of the small intestine and the right lung was homogenized in 1.0 mL Trizol (Life Technologies) and centrifuged at 1,000×g for 5 minutes. RNA was extracted per manufacturer; briefly, 200 µL chloroform was added to the samples and vortexed. After a short incubation, the samples were centrifuged for 15 minutes at 12,000×g at 4 °C. The aqueous phase was transferred to a new Eppendorf tube and 500 µL isopropanol was added. After a 10-minute incubation, the samples were centrifuged at 4 °C at 12,000×g for 10 minutes. The pellet was resuspended in 75% ethanol and vortexed before centrifugation at 4 °C at 7,500×g for 5 minutes. The pellet was then resuspended in 30 µL RNase-free water and incubated at 55 °C for 15 minutes. RNA was then stored at -80 °C until use. Sequencing was performed by the Genome Technology Access Center at McDonnell Genome Institute (GTAC@MGI) at Washington University in St. Louis School of Medicine, USA. RNA sequencing libraries were generated using Clontech SMART-Seq v4 Ultra Low Input RNA Kit for sequencing and Illumina Nextera XT DNA Library preparation kit following the manufacturer's protocol. The cDNA libraries were validated using KAPA Biosystems primer premix kit with Illumina-compatible DNA primers and quality was examined using Agilent Tapestation 2200. cDNA libraries were prepared from RNA samples using PolyA selection, and processed cDNA was sequenced on the Illumina NovaSeq S4 platform (paired-end 150bp reads), generating an average of 36.3 million read pairs per sample (see Supplementary Table S1).

2.6 RNA-seq differential expression analysis

After RNA-seq samples were sequenced, the downloaded reads were trimmed for length and adapters using Trimmomatic v0.36 (22). Then, the reads were aligned to the golden hamster genome assembly [MesAur1.0, downloaded from ENSEMBL (23)] using the STAR aligner (24) (2-pass mode, basic). Of the fifty-six samples, six RNA-seq samples failed QC and were excluded from analysis. Samples sizes were N = 4 for 9 groups, N = 3 for 4 groups, and N = 2 for the day 6, CoV intestine group. Significantly differentially expressed genes between each infected cohort compared to the uninfected cohort was identified using DESeq2 (version 1.12.3) (25) with default settings, using scripts previously provided on Protocol

Exchange (26). Significantly differentially expressed genes (DEGs) were identified based on an FDR-adjusted P value \leq 0.01, a minimum 2-fold change, and expression detected in at least two samples in the higher-expressed group. Additional analysis between infected cohorts was performed at either 3 or 6 days, but not between days of infection. Differentially expressed gene sets compared to the naive cohort were compared across the different infection cohorts, identifying infection-specific and infectionconserved genes and genes differentially expressed only with coinfection with both the worm and the virus across both time points (3 and 6 days after virus infection). Sample metadata and corresponding NCBI SRA accessions (27) are provided in Supplementary Table S1, and complete expression data and differential expression statistics for all genes in all comparisons are provided in Supplementary Table S2. Heatmaps were calculated and visualized in MS Excel, and swarm plots were generated using GraphPad PRISM. Some components of Figures 1-7 were generated in BioRender (citation Rosa, B. 2025 https://BioRender.com/ jwe4naf). Sets of differentially expressed genes (DEGs) were compared and filtered using MS Excel.

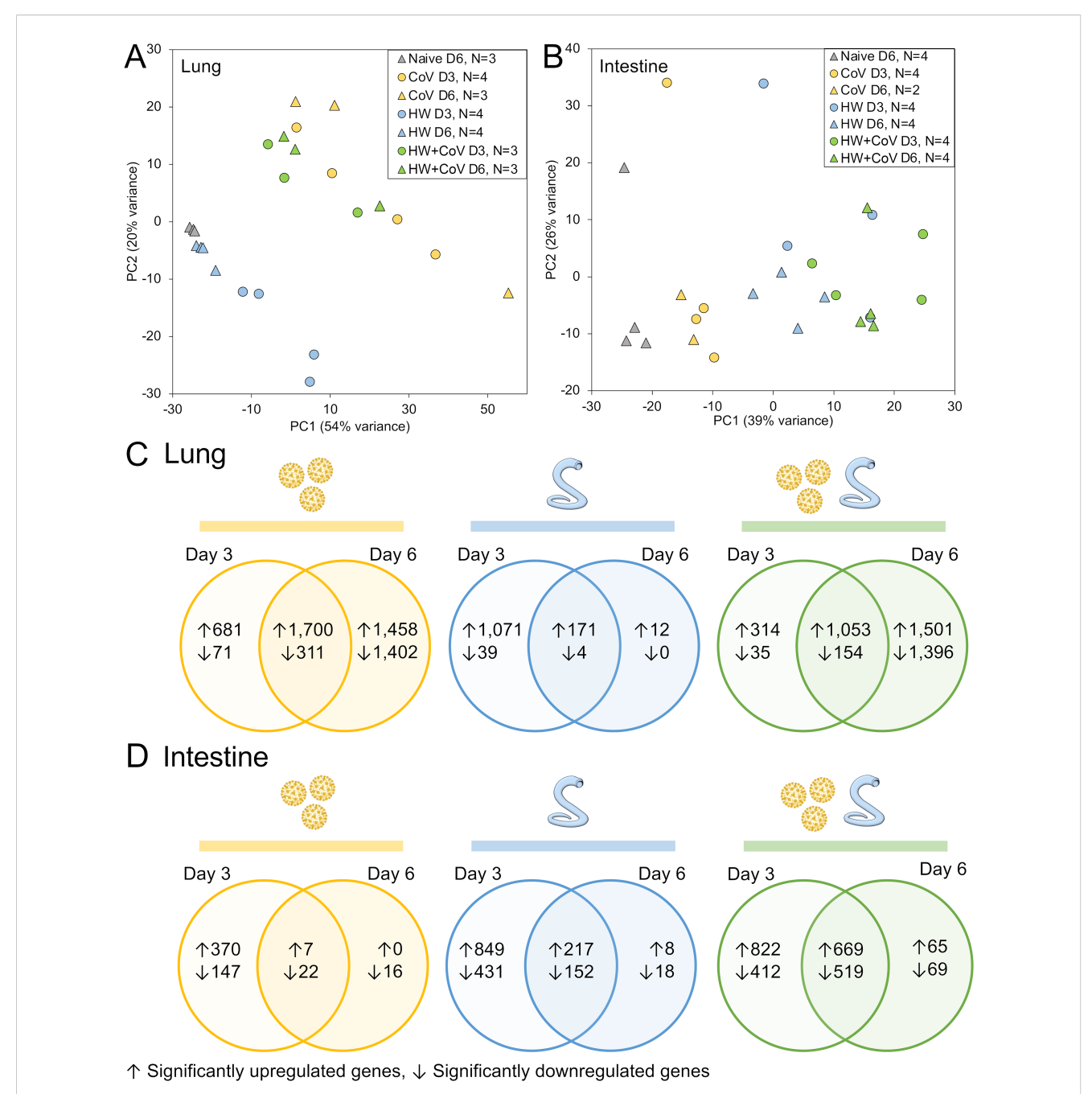
Genes from the hamster genome were assigned putative functional annotations using KEGG (28) and InterProScan (29), and orthology to human genes was identified using annotations from ENSEMBL (23). Pathway enrichment was performed with ShinyGO 0.80 (30), using ENSEMBL (23) annotations for gene ontology biological process terms (31) and KEGG pathway enrichment (28). For all enrichment testing, FDR-adjusted P values ≤ 0.05 were used to identify significant enrichment.

2.7 CIBERSORTx estimation of relative leukocyte cell abundance

Reciprocal best-hit BLAST (32) (NCBI blastp, v2.7.1+) orthologs between hamster proteins and human proteins were identified based on Ensembl genome annotations [MesAur1.0 and GRCh38.112, respectively (23)]. The relative gene expression values of these 1:1 orthologs were used to estimate the relative abundance of 22 leukocyte cell types by performing gene expression deconvolution with the CIBERSORTx (33) algorithm, using the validated "LM22" leukocyte gene signature matrix (34).

3 Results and discussion

This study investigated the impact of prior worm infection on SARS-CoV-2 infection in a Syrian hamster model. Syrian hamsters are considered one of the best animal models for SARS-CoV-2 due to susceptibility to virus infection, ability to transmit the virus, and similarities in disease progression, virus tropism, and severity to humans (35, 36). Syrian hamsters are also susceptible to the hookworm (*Ancylostoma ceylanicum*), which also infects humans as well as other mammals such as dogs and cats. To assess the impact of hookworm infection on SARS-CoV-2 infection and disease, eight groups of age-matched 5–6 week old male hamsters

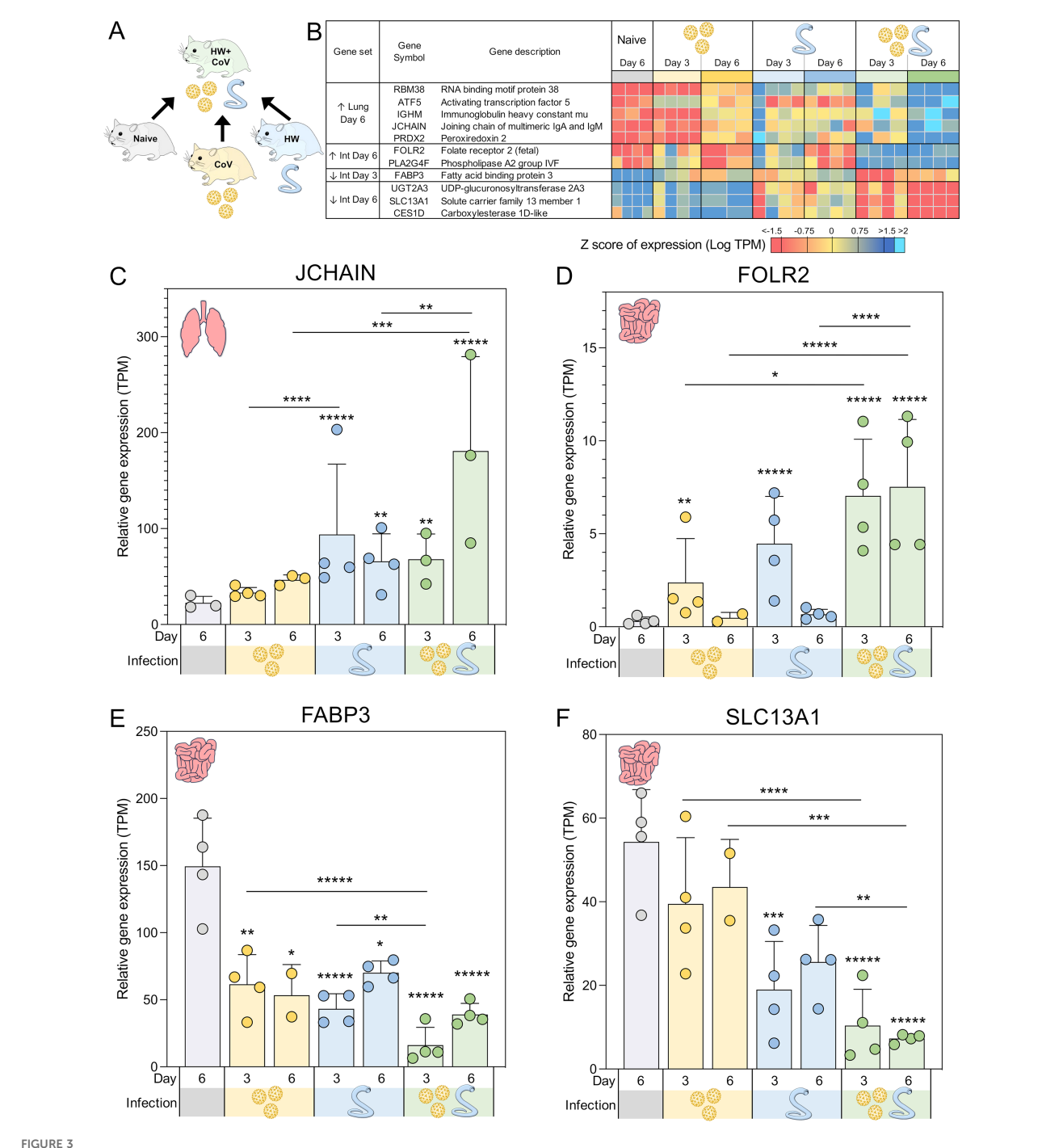


RNA-seq analysis overview. Principal components analysis (PCA) depicting (A) lung and (B) intestine RNA-seq sample similarity based on overall transcriptome profiles, according to DESeq2 analysis, based on sample groups as described in Figure 1A. Sample counts are shown after quality control filtering of RNA-seq sample sets. According to the DESeq2, significantly differentially expressed genes (DEGs) are counted and intersected at the two timepoints for each sample cohort (CoV=yellow, HW=blue, HW+COV=green) in (C) the lungs and (D) the intestines of the hamsters following infection, compared to the Naive cohort.

were infected under different conditions and sacrificed at two timepoints each (three and six days post SARS-CoV-2 infection; Figure 1A) with four infection regimes: (i) Gavaged with PBS (uninfected; Naive), (ii) Gavaged with 80–100 L3 *A. ceylanicum* larvae, and inoculated with PBS 20 days later (hookworm-infected, HW), (iii) Gavaged with PBS and inoculated with 10,000 infectious units of SARS-CoV-2 (WA1/2020) 20 days later (SARS-CoV-2 infected; CoV) and (iv) Gavaged with 80–100 L3 *Ancylostoma*

ceylanicum larvae and inoculated with SARS-CoV-2–20 days later ("coinfected"; HW+CoV).

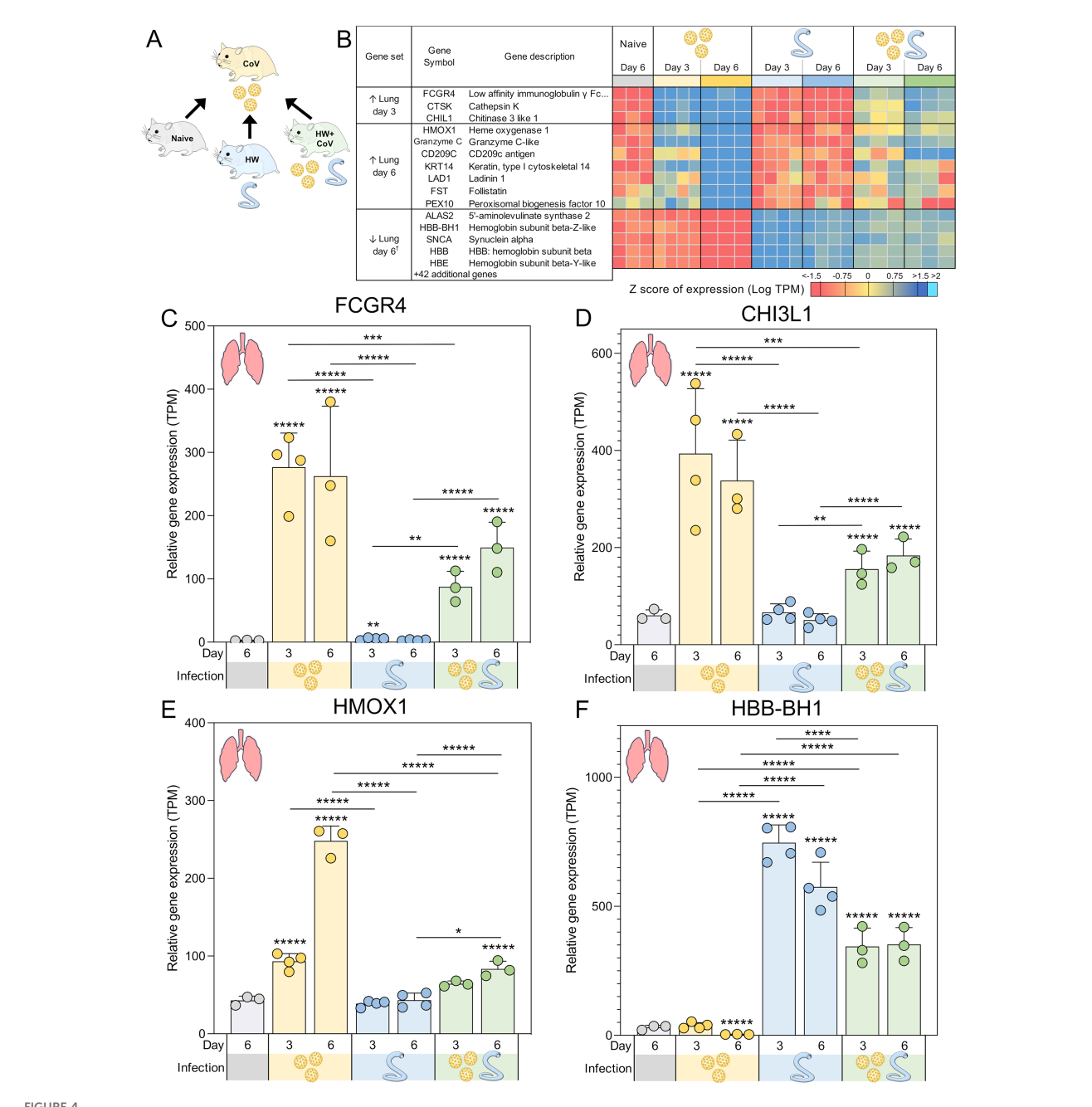
Six days after SARS-CoV-2 infection, naive hamsters increased in weight by an average of 5.8% of their starting weight compared to before infection, while HW caused a decrease in body weight of 1.9% (P = 0.034; Figure 1B). SARS-CoV-2 and coinfection resulted in a 15.0% and 16.5% decrease, respectively (P = 0.0003 and P = 0.0002), similar to weight loss reported in previous SARS-CoV-2-



Genes significantly differentially expressed during coinfection vs all other sample groups. (A) Schematic of the cohorts being compared, with the HW +CoV coinfection cohort being compared to the other three cohorts, for every tissue and timepoint. (B) Heatmap representation of the expression levels of the DEGs of the coinfection group vs all other sample groups in the lungs and intestine (Int). Genes are sorted by FDR-adjusted DESeq2 P values. Swarm plot representations of differential expression are shown for (C) JCHAIN, (D) FOLR2, (E) FABP3 and (F) SLC13A1, which are genes of interest from panel B, with DESeq2 FDR-corrected P values for significance indicated (* $P \le 0.05$, ** $P \le 0.01$, **** $P \le 10^{-3}$, ***** $P \le 10^{-4}$.***** $P \le 10^{-4}$. Asterisks directly above a series indicate significance vs. the uninfected control cohort (grey). Comparisons between infected cohorts were tested on the same days only (i.e., days 3 and 6 are not compared to each other).

infected Syrian hamsters of similar age [e.g. 7.9 to 15.4% (35), 10 to 17% (37), 4 to 15% (38)]. In the lungs of CoV and HW+CoV hamsters, high viral RNA titers were detected on day 3 (\sim 8.9×10⁷ PFU/mL and 1.0×10^8 for CoV and HW+CoV groups respectively) and substantially reduced by day 6 post infection (1.0×10^4 and

 5.6×10^4 PFU/mL; Figure 1C), with no significant difference observed between the two groups. Similar results were obtained for the nasal turbinates (day 3: 1.4×10^7 PFU/mL for CoV and 1.0×10^7 PFU/mL for HW+CoV; day 6: 1.4×10^3 PFU/mL for CoV and 1.3×10^3 PFU/mL for HW+CoV; Figure 1D), also in agreement

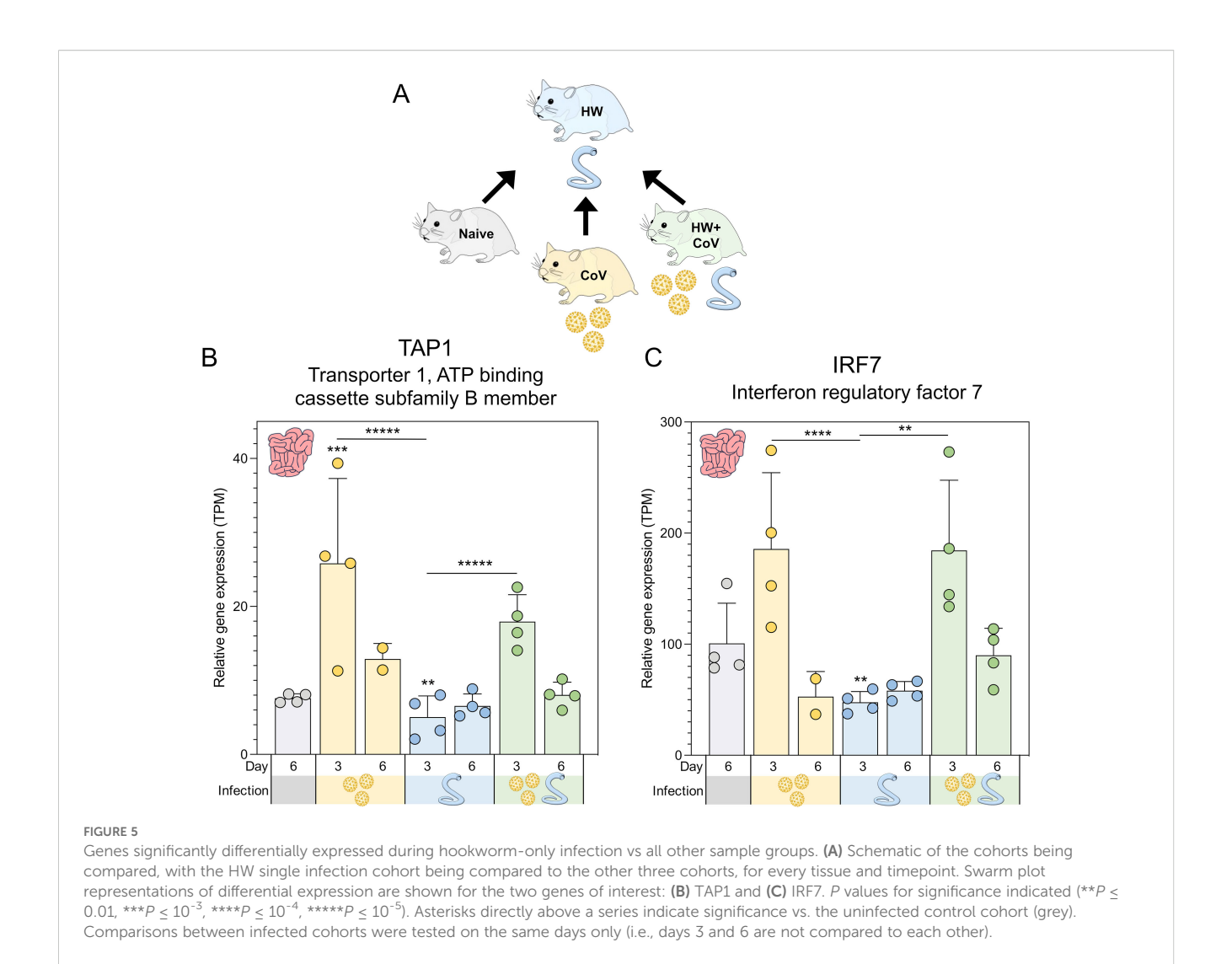


Genes significantly differentially expressed during SARS-CoV-2-only infection vs all other sample groups. (A) Schematic of the cohorts being compared, with the CoV single infection cohort being compared to the other three cohorts for every tissue and time point. (B) Heatmap representation of the expression levels of gene sets significantly upregulated or downregulated between the SARS-CoV-2-only group and all other sample groups in the lungs. Genes are sorted by DESeq2 FDR-adjusted P values. Swarm plot representations of differential expression are shown for (C) FCGR4, (D) CHI3L1, (E) HMOX1 and (F) HBB-BH1, which are genes of interest from panel B, with DESeq2 FDR-corrected P values for significance indicated (* $P \le 0.05$, ** $P \le 0.01$, *** $P \le 10^{-3}$, **** $P \le 10^{-4}$, ***** $P \le 10^{-5}$). Asterisks directly above a series indicate significance vs. the uninfected control cohort (grey). Comparisons between infected cohorts were tested on the same days only (i.e., days 3 and 6 are not compared). [†]Top five most significant of 47 total genes shown.

with previously-published studies (e.g. $\sim 1 \times 10^7$ at day 3, $\sim 1 \times 10^3$ at day 6 (35, 39)).

Despite no changes in weight loss or virus titers between the CoV and HW+CoV hamsters, differences in host responses to the infection may still occur. To assess the impact of hookworm infection on the host response to SARS-CoV-2 infection (and vice versa), RNA was extracted from the lungs and intestine of each

hamster at the timepoint coinciding with 3 or 6 days post-infection with SARS-CoV-2 (Figure 1A), and RNA-seq datasets were generated by Illumina sequencing, generating an average of 55.8 million read pairs per sample (sample metadata and corresponding NCBI SRA accessions (27) provided in Supplementary Table S1). Samples clustered according to their overall transcriptome profile generally by cohort according to principal component analysis

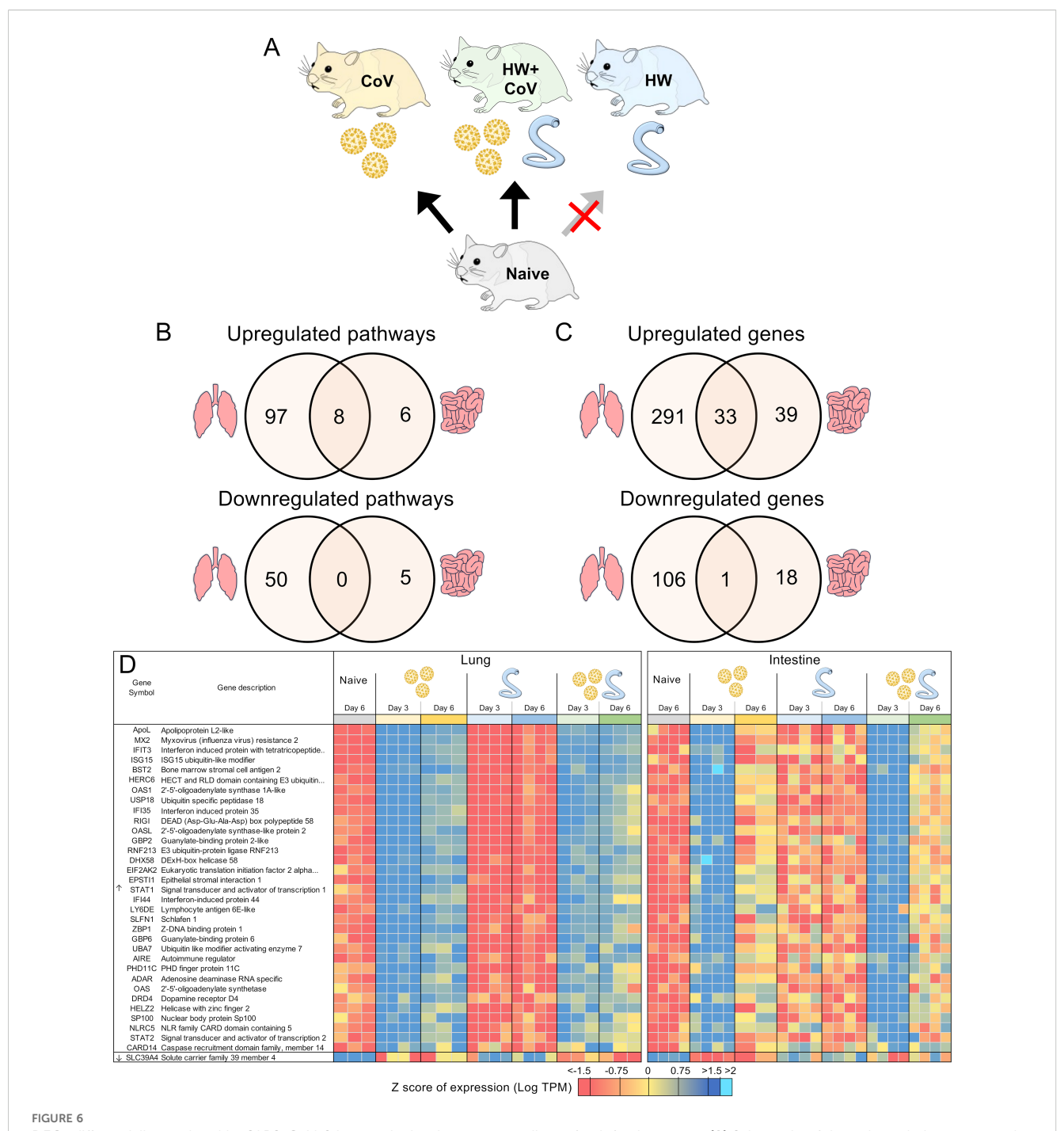


(PCA), for both the lung (Figure 2A) and the intestine samples (Figure 2B). Differential gene expression analysis was performed using DESeq2 (25), with significantly differentially expressed genes (DEGs) requiring an FDR-adjusted P value \leq 0.01, a minimum 2-fold change, and expression detected in at least two samples in the higher-expressed group. Supplementary Table S2 contains lists of DEGs, relative abundance, and differential expression statistics for all genes and all comparisons, which include each infected cohort vs the naive cohort in the same tissue and the infected cohorts compared to each other in the same tissue on the same day.

Following SARS-CoV-2 infection (CoV cohort), 1,700 DEGs were consistently (day 3 and day 6) upregulated (Figure 2C), and 311 were downregulated in the lung, compared to only 7 and 22 DEGs (respectively) in the intestine (Figure 2D), which may be expected since CoV primarily infects the lungs, with very low loads in the intestine that are probably cleared up by day 6 (40). Likewise, HW only infects the intestine and results in more consistent DEGs in the intestine (217 upregulated, 152 downregulated) compared to the lungs (171 and 4, respectively). With HW+CoV coinfection, 1,053 DEGs were upregulated, and 154 were downregulated in the

lung compared to 669 and 559 (respectively) in the intestine. In the lungs, differential gene expression counts were higher at day 6 for CoV-infected cohorts, but higher at day 3 in the HW cohort (Figure 2C), while in the intestine, more genes were differentially expressed at day 3 than at day 6 in all infection cohorts (Figure 2D).

Pathway enrichment was performed with ShinyGO 0.80 (30) for each set of DEGs to identify significantly enriched gene ontology biological process terms (31) and KEGG pathways (28). The number of significantly enriched pathways among the sets of DEGs compared to the naive controls (as described above) are summarized in Supplementary Figure S1. As expected, in the lungs, the "Coronavirus disease-COVID-19" KEGG pathway (maua05171) was significantly enriched among DEGs upregulated in HW+CoV vs both naive and HW at both days ($P \le 1.8 \times 10^{-5}$ in all four comparisons), but not vs the CoV cohort. However, no pathways were significantly enriched in the lungs among all three sets of DEGs as outlined in Figure 3A. In the subsections below, both specific differentially expressed genes and pathway enrichment among the larger sets of DEGs will be described in each comparison in order to thoroughly explore the results.



DEGs differentially regulated by SARS-CoV-2 but not by hookworm, regardless of coinfection status. (A) Schematic of the cohorts being compared: The comparison indicated by the red X must not be significant for genes to be considered. (B) Intersections of pathways of interest enriched among sets of DEGs in both the lung (at both day 3 and day 6) and the intestine (at day 3). (C) Intersections of DEGs of interest in both the lung (day 3 and day 6) and the intestine (day 3). (D) Heatmap representation of the expression levels of gene sets from the intersections of the Venn diagrams from panel (C) Genes are sorted by DESeq2 FDR-adjusted *P* values.

Counts of DEGs and the number of enriched pathways for each set of DEGs are provided in Supplementary Table S3, and FDR-adjusted *P* values for significance for all enriched pathways in all sets of DEGs are provided in Supplementary Table S4, with parsed pathways of interest provided in Supplementary Table S5. Details of sets of DEGs and enriched pathways are described in the sections below.

3.1 Genes uniquely upregulated in the lungs of coinfected hamsters at day 6 are associated with B cell immunity

To identify coinfection-specific gene transcriptional signatures, we identified DEGs in the HW+CoV cohort relative to the other three cohorts (naive, CoV, and HW; Figure 3A) at day 3 and day 6

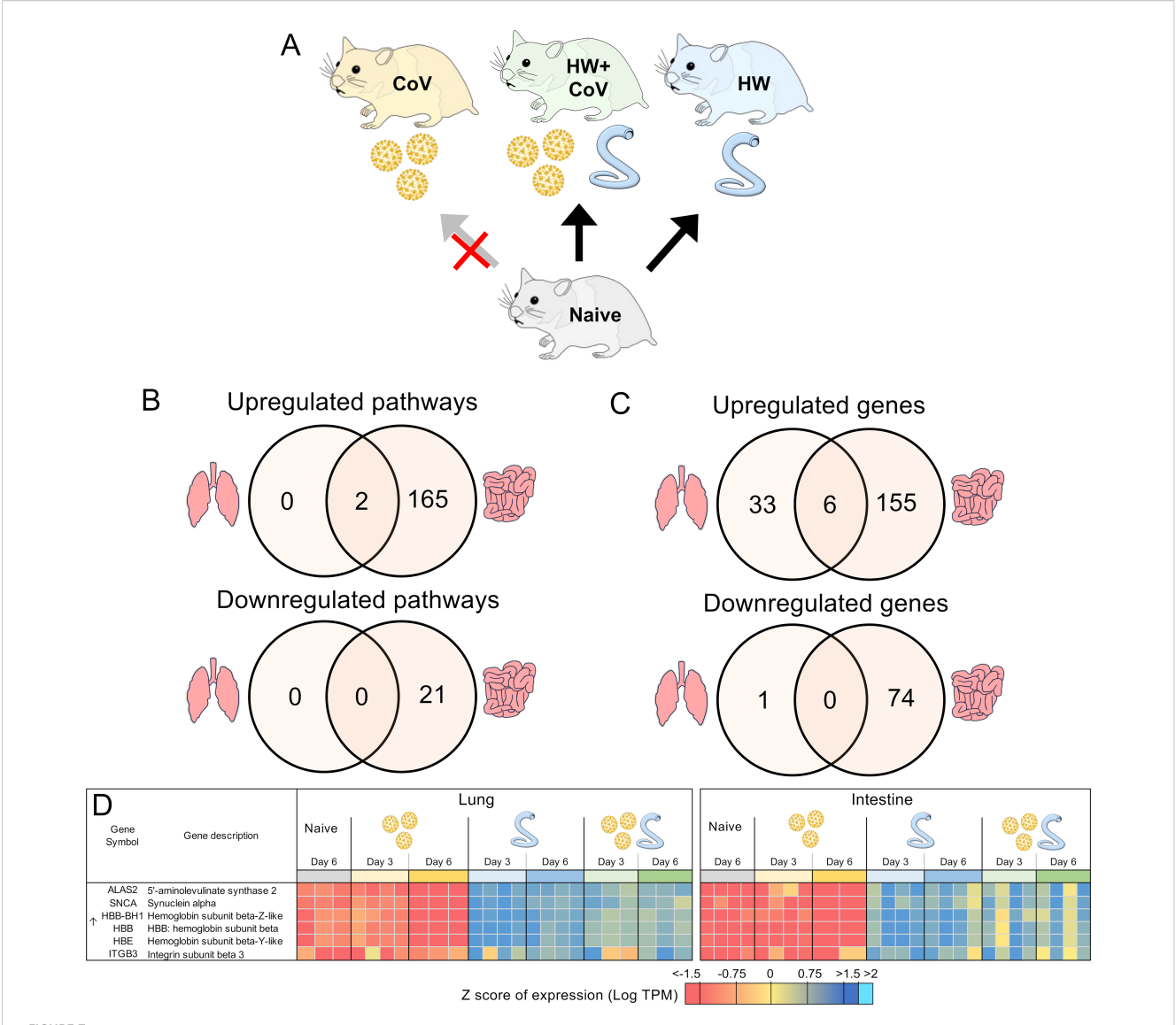


FIGURE 7
Genes differentially regulated by hookworm but not by SARS-CoV-2, regardless of coinfection status. (A) Schematic of the cohorts being compared: The comparison indicated by the red X must not be significant in order for genes to be considered. (B) Intersections of pathways of interest enriched among sets of DEGs in both the lung (left) and the intestine (right), at both day 3 and day 6. (C) Intersections of DEGs in both the lung and the intestine, at both day 3 and day 6. (D) Heatmap representation of the expression levels of gene sets from the intersections of the Venn diagrams from panel (C) Genes are sorted by FDR-adjusted P values.

in the lungs and in the intestine, ensuring that differential expression was very specific to coinfection as opposed to single CoV or HW infections. DEGs were categorized by differential regulation direction (higher/upregulated or lower/downregulated), time point (day 3 or 6) and tissue (lung or intestine).

Five DEGs were significantly higher in the lungs of the HW +CoV cohort compared to each of the other cohorts on day 6 (Figure 3B). These included *RBM38* (RNA binding motif protein 38), which was significantly upregulated at day 6 in both individual infections but even more significantly upregulated at day 6 in the coinfection cohort. *RBM38* is essential for proper hematopoiesis

(41) and belongs to a class of proteins that includes RMB24, which inhibits the translation of SARS-CoV-proteins by targeting single or double-stranded regions of RNA molecules (42). Three of these genes were not upregulated by day 6 in either of the single infections: (i) ATF5 (Activating transcription factor 5), which regulates B cell survival during stress (43) and has roles in cellular differentiation (44); (ii) IGHM (Immunoglobulin heavy constant mu), which plays an important role in the neutralization of SARS-CoV2 (45); and (iii) PRDX2 (Peroxiredoxin 2), which serves as the primary antioxidant in erythrocytes, effectively neutralizing hydrogen peroxide generated endogenously through

hemoglobin autoxidation (46). The extent of PRDX2 oxidation is notably elevated in various pathological conditions, making it a potential biomarker for oxidative stress. Finally, *JCHAIN* (Joining chain of multimeric IgA and IgM) was significantly upregulated in the lungs of HW but not the CoV hamsters at day 6, but was far more significantly upregulated in the HW+CoV cohort (Figure 3C). JCHAIN regulates the multimerization of secretory IgM and IgA and is required for their transport across the mucosal epithelium (47, 48). Immunoglobulin-A (IgA), the "mucosal Immunoglobulin," has been a focal point in the study of SARS-CoV-2 immunity, diagnosis, and immunization (49).

Overall, the upregulation of these specific genes at day 6 indicates that coinfection with HW+CoV leads to an increase in hematopoiesis (*RBM38*) and B cells (*ATF5*), as well as an increase in *IgM* and *JCHAIN* which are both produced and secreted by B cells, with important roles in COVID-19 immunity. These results suggest that pre-infection with hookworm may produce a more robust B cell response in the lungs of infected animals by day 6.

3.2 Genes uniquely differentially regulated in the intestine of coinfected hamsters are associated with inflammation

Several pathways were significantly enriched in the intestine among all three sets of coinfection DEGs, as outlined in Figure 3A (pathways listed in Supplementary Table S5A). On day 3, 11 GO terms related to immune responses and 2 related to stress responses were significantly enriched among upregulated DEGs, and 3 terms related to lipid transport were enriched among downregulated DEGs. This indicates an increase in overall immune and stress response activations corresponding with lipid metabolism downregulation in the intestine due to coinfection compared to single infections. On day 6, overall metabolic pathways and specific metabolism of retinol, xenobiotics, ascorbate, and aldarate were downregulated.

Two genes were significantly upregulated in the intestines of the coinfection cohort compared to all other sample groups in the intestine on day 6, and both were not significantly upregulated at day 6 in either of the single infections: (i) FOLR2 (Folate receptor 2; Figure 3D), which is a glycosylphosphatidylinositol-anchored glycoprotein that is predominantly expressed by monocytes and macrophages (50). FOLR2 isoform FRβ is upregulated in activated macrophages during acute inflammation resulting from the pathogenesis of various human inflammatory diseases, suggesting a role in this receptor in macrophage-controlled inflammation regulation (50). This is consistent with research showing a role for folate in regulating inflammatory responses including those induced by pathogen-associated molecular patterns (PAMPs) such as lipopolysaccharide (LPS) (50-52); (ii) PLA2G4F (Phospholipase A2 group IVF, $cPLA2\zeta$), which has a primary known role in mediating arachidonic acid release (53) including from fibroblasts (54) ([which play significant roles in tissue maintenance and immune homeostasis during inflammation and damage in the intestine (55)]. Arachidonic acid and its derivatives play a critical role in inducing inflammation in the intestine, including in diseases such as Crohn's disease and ulcerative colitis (56), which suggests a possible mechanism for PLA2G4F regulation of intestinal inflammation. Another Phospholipase A2 family gene, *sPLA2-IB*, is upregulated by intestinal epithelial cells during nematode infection, and is necessary for their expulsion from the intestine due to its activity in hydrolyzing worm phospholipids (57). While no such activity has been demonstrated for PLA2G4F, this suggests other possible mechanisms for Phospholipase A2 activity against pathogenic infection in the intestine. The upregulation of both *FOLR2* and *PLA2G4F* in the intestine in response to HW+CoV may suggest a mechanism for increasing intestinal inflammation.

One gene, *FABP3* (Fatty acid binding protein 3), was significantly downregulated in the intestines of both the single infections but was much more significantly downregulated in the coinfection cohort compared to all other sample groups in the intestine on day 3 (Figure 3E). *FABP3* is a negative regulator of inflammation in the skin, so its significant downregulation in this dataset may be linked to increased inflammation in the intestine (58). However, FABP3 is typically studied for its roles in heart muscle tissue, while FABP2 is more typically described in the intestine, with SARS-CoV-2 infection having been shown to reduce circulating FABP2, correlating with systemic inflammation (59). In that study, *FABP3* followed a similar expression to *FABP2* but did not reach significance in the same comparisons.

Three genes were significantly lower in the coinfection cohort's intestines than all other sample groups in the intestine on Day 6. The first, UGT2A3 (UDP-glucuronosyltransferase 2A3), was significantly downregulated at day 6 in the HW cohort but was much more significantly downregulated in the coinfected cohort. UGT2A3 is not well-characterized but has been shown to deactivate bacterial-derived intestinal hyodeoxycholic acid (60), which has been shown to attenuate inflammation by targeting the TLR4/MD2 complex (61). The other two genes in this set were not significantly downregulated in either of the single infections: (i) SLC13A1 (Solute carrier family 13 member 1; NAS1), which mediates sulfate absorption across small intestinal epithelia (62) (Figure 3F). NAS1 knockout mice with subsequent intestinal sulfomucin content showed enhanced intestinal permeability and enhanced DSSinduced colitis (63), so its downregulation may be associated with increased intestinal inflammation as well; (ii) CES1D (Carboxylesterase 1D-like), which increases LPS-induced inflammation in the lungs (64), and which is primarily involved in lipid metabolism (65). In the intestine, lipid mediators derived from polyunsaturated fatty acids play complex roles in inflammatory processes (66), so the downregulation of CES1D may indirectly affect inflammation in a similar manner to UGT2A2 and hyodeoxycholic acid.

Taken together, the differential regulation of intestinal genes, specifically with coinfection, may reflect causes of or the responses to intestinal inflammation, indicative of inflammatory reactions in the gut of coinfected hamsters, and were not observed in hamsters infected with either pathogen alone.

3.3 Genes consistently upregulated in the lungs only in SARS-CoV-2-infected hamsters reveal immune responses attenuated by pre-infection with hookworm.

Several gene sets were identified that were differentially expressed in the lungs of the CoV cohort compared to coinfected (HW+CoV) hamsters (Figures 4A, B). Many of these genes (e.g., Figures 4C–E) were strongly upregulated by CoV alone but showed significantly weaker upregulation in the HW+CoV cohort, suggesting that hookworm coinfection attenuated these responses. In other cases (e.g., Figure 4F), genes that were downregulated by CoV were upregulated in HW+CoV, but significantly less upregulated than HW alone.

Three genes were significantly higher in the lungs of the CoV cohort compared to each of the other cohorts on day 3, representing an attenuation of the upregulation by CoV resulting from preinfection with HW: (i) FCGR4 (Low-affinity immunoglobulin gamma Fc region receptor III-like; Figure 4C), the mouse ortholog of human FCGR3A/CD16 (67), which is the major Fc receptor that mediates uptake of opsonized SARS-CoV-2 in monocytes (68). In individuals infected with the human hookworm Necator americanus, FCGR3A was significantly lower in dendritic cells collected from the blood (69), which may explain its attenuation in coinfected lung samples. Higher FCGR3A expression is also associated with recovery from COVID, compared to Long COVID patients (70); (ii) CTSK (Cathepsin K), which is capable of cleaving SARS-CoV-2 spike protein (71) and when transgenically overexpressed in mouse lungs, is associated with reduced collagen deposition, improved lung function parameters, and resistance to pulmonary fibrosis (72). CTSK also contributes to intestinal homeostasis and tissue architecture, with its reduction being associated with higher collagen IV and laminin in the mouse intestine, suggesting a potential interaction with hookworm infection (73); (iii) CHIL1 (Chitinase 3 like 1; CHI3L1; Figure 4D), which is associated with poorer prognosis for patients with SARS-CoV-2 infection (74), and may exacerbate associated lung damage and inflammation by stimulating ACE2 and proteases that prime the viral spike SARS-CoV-2 protein (75). Impaired TH2 responses were observed in CHI3L1 knockout (-/-) mice infected with the intestinal helminth Heligmosomoides polygyrus (76). In the intestine, CHI3L1 is secreted from colonic epithelial cells and its expression exacerbates intestinal inflammation (77), but hookworm infection, conversely, is associated with a reduction of intestinal inflammation, and is considered a potential therapeutic for a range of inflammatory diseases (78). This may suggest that the attenuation of CHI3L1 expression in SARS-CoV-2-infected lungs of coinfected hamsters may reflect the anti-inflammatory effects of hookworm infection, which may lead to better SARS-CoV-2 outcomes.

On day 3 in the lungs, two related KEGG pathways were significantly enriched among the three sets of DEGs in

Figure 4A: Rheumatoid arthritis (maua05323) and Toll-like receptor (TLR) signaling pathway (maua04620; Supplementary Table S5B); TLRs contributes to SARS-CoV-2 clearance and disease resolution, with important roles in inflammatory regulation (79).

At day 6, seven genes were significantly higher in the lungs of the CoV cohort compared to all other sample groups: (i) HMOX1 (Heme oxygenase 1; HO-1; Figure 4E), which confers protection from inflammatory conditions through the removal of heme in tissues including the lungs (80), and has been suggested as an important predictor of COVID-19 severity (81). Upregulation of HMOX1 has been suggested as a promising target for the treatment and prevention of SARS-CoV-2 (82); (ii) Granzyme C-like, which is predominantly synthesized by mouse CD4+ and CD8+ T cells under in vitro conditions or during mixed lymphocyte reactions (83). Granzymes including the human ortholog of Granzyme C-like (Granzyme B) have the capability to directly inhibit viruses by inducing proteolysis of viral or host cell proteins necessary for the viral entry, release, or intracellular trafficking, and by augmenting pro-inflammatory antiviral cytokine responses (84); (iii) CD209C (Cluster of Differentiation 209; also called Dendritic Cell-Specific Intercellular Adhesion Molecule-3-Grabbing Non-integrin, DC-SIGN), is a type C lectin found on alveolar macrophages and dendritic cells, which plays a key role in innate immunity and antiviral defense by acting both as a pathogen recognition receptor and a cell adhesion receptor (85). It can bind various microorganisms including SARS-CoV-2, and its polymorphisms are significantly associated with an increased risk of COVID-19 infection (85); (iv) KRT14 (Keratin, type I cytoskeletal 14), the expression of which can serve as a marker for lung regeneration and repair during alveolar damage (86); (v) LAD1 (Ladinin-1; Leukocyte adhesion deficiency-1), which is expressed in squamous and glandular epithelia, with a well-established function as an anchoring filament protein. LAD-1 plays a critical role as a component of the basement membrane zone and is negatively correlated in lung cancer survival (87); (vi) FST (Follistatin), which is associated with COVID-19 mortality (88) and severe Long Covid (89) and (vii) PEX10 (Peroxisomal biogenesis factor 10), which is critical for peroxisomal matrix-protein import (90), but has no previously described associations with SARS-CoV-2 infection.

Overall, these data indicate that certain host genes and pathways strongly upregulated by CoV infection become attenuated or even reversed when hamsters are pre-infected with HW. The DEGs include many known biomarkers of COVID-19 severity and outcomes, highlighting the importance of considering coinfections when evaluating transcriptional signatures of infection. The enrichment of TLRs additionally highlights the capacity of hookworm infection to reshape the antiviral inflammatory response. Consequently, hookworm-induced immune regulation may reduce lung inflammation and potentially improve SARS-CoV-2 outcomes, pointing to broader implications for helminth-viral coinfections.

3.4 Genes with attenuated or reversed SARS-CoV-2-induced downregulation in the lung during coinfection with hookworm include enrichment of hemoglobin b genes

A total of 47 genes were significantly lower in the lungs the CoV cohort compared to all other sample groups in the lung at day 6 (The top five are shown in Figure 4B), indicating attenuated downregulation responses with in the HW+CoV cohort. All four Syrian hamster hemoglobin b genes were among these 47 (HBB-BH1 [Figure 4F], HBE, HBB-Y, and HBB; FDR-adjusted enrichment $P = 1.8 \times 10^{-7}$ for IPR002337). SARS-CoV-2 binds to red blood cell progenitors and dysregulates hemoglobin metabolism (91), but HW infection is known to be negatively associated with Hb concentrations in the blood (92), likely due to their blood feeding, so increased expression of these genes may indicate compensation by the host to regenerate Hb. The genes among this group that were the most significantly downregulated by CoV at day 6 also included AOC3 (Amine Oxidase Copper Containing 3; VAP-1), which is dramatically increased in expression in severe COVID-19 cases but downregulated during the convalescent stage (93) and IGFBP3 (Insulin-like growth factor binding protein 3), which was downregulated in severe and critical COVID-19 patients (94). The 47 genes were significantly enriched for oxygen transport (GO:0015671, $P = 3.3 \times 10^{-6}$), possibly due to adaptations to HWinduced anemia.

3.5 Genes with reversed hookworminduced downregulation in the intestine during coinfection with SARS-CoV-2 are both related to Type I interferon

Two genes were significantly lower in the intestines of the HWonly cohort compared to all other sample groups at day 3 (Figure 5A): (i) TAP1 (Transporter 1, ATP binding cassette subfamily B member; Figure 5B) is a membrane-bound protein composed of two membrane-spanning domains and belongs to the ATP-binding cassette (ABC) transporter superfamily, playing a critical role in transporting antigens from the cytoplasm to the endoplasmic reticulum, where it interacts with major histocompatibility complex (MHC) class I molecules (95) and (ii) IRF7 (Interferon regulatory factor 7; Figure 5C), which is recognized as the master regulator of type I IFN production (96). Previously, the intestinal helminth H. polygyrus has been shown to modulate RSV lung inflammation and disease through the induction of type I IFN responses mediated through the gut microbiota (10). TAP1 also demonstrates broadly antiviral activities through the activation of type I IFN responses, including IRF3 (97), so these two genes may indicate a shared type I IFN mechanism that is downregulated by HW infection but upregulated during HW+CoV due to the influence of CoV infection on intestine transcription.

3.6 Covid-upregulated genes that are not upregulated by hookworm infection follow expectations for immune responses to COVID-19 infection

In addition to the genes uniquely differentially regulated during coinfection described above, to characterize general SARS-CoV-2 responses, we also identified DEGs consistently differentially regulated by CoV but not by HW (Figure 6A). As expected, many more pathways were significantly enriched among the DEGs in the lungs (Figure 6B), with the top most significantly enriched pathway among lung-upregulated gene sets being "Coronavirus disease-COVID-19" (maua05171; FDR-adjusted $P < 1.9x10^{-5}$ at day 3 and $P < 10^{-35}$ at day 6), and the other top enriched pathways being related to the immune system, inflammatory responses and cytokine production (Supplementary Table S5D). In both the lung and the intestine, 8 pathways were significantly enriched among upregulated DEGs in both CoV comparisons, including "cellular response to cytokine stimulus", "response to interferon-beta," and "NOD-like receptor signaling pathway", while 6 terms, including several terms related to type I interferon were only significantly enriched among the intestine-upregulated DEGs but not the lungs (Supplementary Table S5D). No terms overlapped both tissues among downregulated DEGs (Figure 6B).

In the lungs, there were 324 DEGs upregulated by SARS-CoV-2 both in the CoV and the HW+CoV cohorts, which were not upregulated by HW alone on both days. Because of the low number of genes differentially regulated by CoV in the intestine at day 6 (Figure 2D), the same parsing was performed using only day 3, identifying 72 CoV-specific upregulated DEGs. There were 33 DEGs overlapping these two gene sets between the two tissues, representing systemic upregulated genes spanning tissues (Figure 6C, where the probability of this much overlap is $P < 10^{-15}$ by random chance; binomial distribution test). These 33 genes were enriched for many pathways and functions (Table 1), including 17 genes assigned to "response to biotic stimulus" (GO:009607, FDR-adjusted P =3.6x10⁻¹³) and 6 genes assigned to the "Coronavirus disease-COVID-19" KEGG pathway (maua05171, FDR-adjusted $P = 1.4 \times 10^{-5}$). In order of average DESeq2 significance, these six genes are (i) MX2, an IFN-stimulated gene with broad antiviral activity (98), which correlates with SARS-CoV-2 viral load (99), (ii) OAS1, which protects against SARS-CoV-2 infections via RNase L enzyme activity in humans, and protects against viral infections through non-canonical IFN pathways in both mouse and human (100), (iii) EIF2AK2, which is important for activating IFN responses and interfering with host cell translation during SARS-CoV-2 infection (101), (iv) STAT1, which plays a crucial role in viral infection control, including for SARS-CoV-2 (102), (v) ADAR, which protects against SARS-CoV-2 infection through enhanced T cell responses and reduced viral load (103), and (vi) STAT2, which restricts SARS-CoV-2 dissemination but can drive severe pneumonia in hamsters (104). Other genes among the 33 include interferonrelated genes IFIT3, IFI35 and IFI44. The complete list of 33 genes and their relative expression across both intestine and lung samples

are shown in Figure 6D, and highlights the value of the overall dataset in identifying known SARS-CoV-2 responsive DEGs.

Considering the downregulated DEGs with the same intersection of differential expression across cohorts, we identified 107 lung-downregulated genes and 19 intestine-downregulated genes, with the only intersection between the tissues being the zinc ion transporter gene *SLC39A4* (Figure 6C), which may be involved in accelerating tumor development by impairing immune responses in cytokine signaling pathways and IL-17 signaling pathways (105).

3.7 Hookworm-upregulated genes that are not upregulated by SARS-CoV-2 are associated with hemoglobin

Like the analysis in the previous section, we also identified DEGs that were consistently differentially regulated by HW on both days but not by CoV infection alone (Figure 7A). Only two pathways were consistently significantly enriched in the lungs among the upregulated DEGs (gas transport and oxygen transport), and both of these were also significantly enriched among the upregulated DEGs in the intestine (Supplementary Table S5E), likely compensating for hookworm-induced anemia (106). An additional 167 pathways were enriched among the DEGs upregulated in each comparison in the intestine, the most significant of which were related to cell motility, blood vessel development, and leukocyte activation. Among the DEGs downregulated in each comparison in the intestine, 12 pathways were enriched including pathways related to anion transport, bile secretion and lipid catabolism (Supplementary Table S5E).

In the lungs, 39 DEGs were upregulated by hookworm on both days, both in the HW infection and the HW+CoV cohorts, which were not upregulated by CoV infection alone (Figure 7B). In the intestine, the same parsing identified 161 HW-specific upregulated genes. There were 6 genes overlapping these two gene sets between the two tissues (Figure 7C), representing systemic upregulated genes spanning tissues (where the probability of this much overlap is 5.0x10⁻⁸ by random chance). In order of average DESeq significance, these 6 genes were ALAS2, SNCA, three hemoglobin b genes (HBB-BH1, HBB, HBE), and ITGB3 (Figure 7D). The hemoglobin genes were described above in relation to genes with attenuated or reversed CoV-induced downregulation during coinfection with HW+CoV, highlighting the worm-induced systemic upregulation of these genes despite their significant downregulation in the CoV-only cohorts. The precursor protein of ALAS2 includes motifs responsive to heme, which hinder its translocation into mitochondria upon heme binding (107), and erythropoietic factors and iron availability are the principal regulators influencing ALAS2 (107, 108), so there may be a link to heme with that gene as well.

Among the HW-downregulated genes, 74 were consistently downregulated by HW but not CoV in the intestine, but only one

(*PLK2*; Polo-like kinase2) was consistently downregulated in the lungs. Genetic deletion of *PLK2* in the lungs induces a pro-fibrotic phenotype, suggesting a role in regulating fibrosis (109).

3.8 CIBERSORTx-estimated relative abundance of leukocyte cells in lung samples

The relative gene expression profiles for reciprocal best-hit (1:1) orthologs between hamster proteins and human were used to estimate the relative abundance of 22 leukocyte cell types in the lung samples, using CIBERSORTx (33) (see Methods; Supplementary Table S2; Supplementary Table S6). Both CoV and HW+CoV infection resulted in a significant increase in activated natural killer (NK) cells (from 12.6% to more than 21.1% at both days), but these were significantly reduced with HW alone (8.3%); In previous research, NK cell tissue distribution was found to be affected by CoV infection, and a prompt NK cell response was found to possibly determine a good clinical outcomes (110). M0 macrophages were significantly reduced by both CoV and HW+CoV (from 5.7% to ≤ 1% each), while M1 and M2 macrophages were significantly increased in both of these cohorts [which produce pyrogenic and inflammatory mediators in response to CoV infection (111)]. Additionally, resting mast cells (7.3% in naive) were significantly reduced by CoV and HW+CoV (≤1% each), while activated mast cells increased but not significantly in these cohorts; Activation of mast cells is a potential biomarker for CoV infection, and activation profiles are associated with severe outcomes (112). Relative to CoV, only memory B cells were significantly higher in HW+CoV, at day 3 (2.6% vs 0.4%; FDR-corrected P = 0.021). Overall, these results suggest that, with the exception of memory B cells, leukocyte cell recruitment responses to CoV are not substantially affected by prior HW infection, despite the differential activation of many genes and pathways as described above.

4 Conclusion

Our study provides insights into how concurrent hookworm and SARS-CoV-2 infections affect host transcriptional responses across the lung and intestine, shedding light on potential immunological interactions between these pathogens. Our dataset included RNA-seq samples generated from lung and intestinal tissue from cohorts of naive, CoV-infected, HW-infected, and HW+CoV hamsters collected at two-time points (3 days and 6 days post-infection with CoV). Each of the infected cohorts showed significantly reduced weight compared to naive, and virus titers were similar for CoV and HW+CoV cohorts, lowering by several orders of magnitude between day 3 and day 6. This experimental design facilitated several strategies for intersecting DEG sets of interest to analyze different aspects of the host response to infection.

Consistent transcriptional differences were observed in the coinfection cohort compared to naive and single-infection

TABLE 1 Significantly enriched Gene ontology terms and KEGG pathways among the 33 genes consistently upregulated by SARS-CoV-2 infection (alone or during coinfection), but not by hookworm alone, in both the lung and the intestine.

Database	Pathway id	Description	Total term size	# in gene set	FDR-adjusted <i>P</i>
Gene Ontology (BP) (Top 15 shown)	GO:0009607	Response to biotic stimulus	757	17	3.5×10 ⁻¹³
	GO:0051707	Response to other organism	727	17	3.5×10 ⁻¹³
	GO:0098542	Defense response to other organism	495	15	3.5×10 ⁻¹³
	GO:0044419	Biological proc. involved in interspecies interaction	814	17	9.2×10 ⁻¹³
	GO:0009615	Response to virus	217	11	1.1×10 ⁻¹¹
	GO:0051607	Defense response to virus	156	10	1.3×10 ⁻¹¹
	GO:0140546	Defense response to symbiont	157	10	1.3×10 ⁻¹¹
	GO:0045087	Innate immune response	300	11	2.5×10 ⁻¹⁰
	GO:0006952	Defense response	847	15	3.5×10 ⁻¹⁰
	GO:0034097	Response to cytokine	488	12	1.7×10 ⁻⁹
	GO:0060337	Type I interferon signaling pathway	33	6	1.7×10 ⁻⁹
	GO:0071357	Cellular response to type I interferon	34	6	1.8×10 ⁻⁹
	GO:0002831	Reg. of response to biotic stimulus	214	9	6.0×10 ⁻⁹
	GO:0009605	Response to external stimulus	1553	17	9.6×10 ⁻⁹
	GO:0060338	Reg. of type I interferon-mediated signaling pathway	28	5	6.6×10 ⁻⁸
KEGG	maua05162	Measles	101	6	9.9×10 ⁻⁷
	maua05164	Influenza A	121	6	1.4×10 ⁻⁶
	maua05171	Coronavirus disease-COVID-19	190	6	1.4×10 ⁻⁵
	maua05160	Hepatitis C	119	5	2.2×10 ⁻⁵
	maua04217	Necroptosis	87	4	1.4×10 ⁻⁴
	maua04621	NOD-like receptor signaling pathway	114	4	3.5×10 ⁻⁴
	maua05165	Human papillomavirus infection	241	5	4.0×10 ⁻⁴
	maua05169	Epstein-Barr virus infection	148	4	7.2×10 ⁻⁴
	maua05168	Herpes simplex virus 1 infection	200	4	2.0×10 ⁻³
	maua05167	Kaposi sarcoma-associated herpesvirus infection	137	3	7.8×10 ⁻³
	maua04623	Cytosolic DNA-sensing pathway	41	2	9.3×10 ⁻³
	maua04625	C-type lectin receptor signaling pathway	82	2	0.033
	maua04380	Osteoclast differentiation	91	2	0.037
	maua04120	Ubiquitin mediated proteolysis	95	2	0.037
	maua04630	JAK-STAT signaling pathway	102	2	0.040
	maua05161	Hepatitis B	113	2	0.045

cohorts, underscoring how helminth-induced immunomodulation can reshape the host response to viral infections. Coinfected hamsters showed distinct transcriptional signatures in the lungs by day 6, including the upregulation of *ATF5*, *IGHM*, and *JCHAIN*, which together with the increase in memory B cells, suggest that prior hookworm infection may enhance B cell-mediated immunity and secretory IgM/IgA pathways in the lungs, to rapidly clear the

virus. Hookworm infection is known to induce robust Th2 responses driven by IL-4 (6, 113, 114).

In the intestine, coinfection resulted in the distinct upregulation of multiple inflammatory and stress-related gene signatures, including *FOLR2* and *PLA2G4F*, which were not significantly upregulated in the single-infection cohorts. These and other coinfection-specific genes point to an intensified inflammatory

state in the gut, possibly reflecting differences in the hookworm's capacity to modulate inflammatory processes during overlapping viral challenges. Pathway enrichment analysis of each set of DEGs also supported the upregulation of stress responses and the downregulation of lipid metabolism pathways in the intestine.

An additional analysis identified several host genes and pathways, including FCGR4, CTSK, HMOX1, and Granzyme C, that are strongly differentially regulated by CoV infection alone and become attenuated or even reversed when hamsters are pre-infected with HW. These shifts in gene expression, including overall enrichment in toll-like receptor signaling, indicate specific targets and pathways that are predisposed to differential responses to CoV with prior HW infection, potentially indicating mechanisms for reduced inflammation and improved CoV infection outcomes. Among the genes with attenuated CoV upregulation when coinfected with HW were previously proposed host protein biomarkers for the prognosis of COVID severity [CHI3L1 (74), HMOX1 (82)], Long COVID [FCG4/FCGR3A (70) and FST (89)] and mortality [FST (88)]; These may indicate key genes involved in the lower COVID outcomes in helminth-endemic regions (12).

Similarly, HW infection suppresses select type I interferonrelated genes (*TAP1* and *IRF7*) in the intestine, but this effect is reversed by CoV coinfection, suggesting a shared IFN-driven antiviral mechanism. In the lungs, DEGs associated with HWonly infection are consistently enriched for the upregulation of oxygen transport and downregulation of many immune system processes, including cytokine production, but these pathways are no longer enriched in the HW+CoV cohort, indicating a reversal of HW-induced immunomodulation in response to CoV infection.

Finally, we observed expected genes and enrichment among DEGs associated with CoV but not HW (including enrichment of the "Coronavirus disease-COVID-19" pathway in the lungs, and cytokine, interferon and NOD signaling pathways in both tissues), and many genes and pathways indicative of HW-induced anemia were differential with HW but not CoV. These results highlight the high quality of the dataset by reproducing expected biological findings and provide an additional resource to data mine for the impact of specific infections on the transcriptome of the lung and the intestine.

Overall, by investigating CoV and HW coinfections and comparing them to naive and single infections, we have successfully identified host responses unique to coinfection, analyzed from several perspectives, including the reversal of infection-induced differential regulation. Given the high prevalence of hookworm and other helminth infections in many resource-limited regions, understanding how these parasites influence the course and severity of viral infections, particularly in the respiratory tract, holds significant public health and clinical relevance. Future work, including functional validation of coinfection-specific targets, evaluation of differences of expression at the protein level, mechanistic studies of helminth-associated immune modulation, and experiments with other helminth species with different tropisms, will help clarify whether targeting

these pathways can reduce severe outcomes in viral respiratory diseases, especially within populations heavily burdened by parasitic infections.

Data availability statement

The datasets presented in this study can be found in online repositories. The names of the repository/repositories and accession number(s) can be found in the article/Supplementary Material.

Ethics statement

All animal experiments were carried out under protocols approved by Washington University School of Medicine Institutional Animal Care and Use Committees (assurance number A3381-01). All housing and care of laboratory animals conformed to the National Institutes of Health (NIH) Guide for the Care and Use of Laboratory Animals in Research (see 18-F22) and all requirements and regulations issued by the United States Department of Agriculture (USDA), including regulations implementing the Animal Welfare Act (P.L. 89-544) as amended (see 18-F23). The study was conducted in accordance with the local legislation and institutional requirements.

Author contributions

BR: Data curation, Formal Analysis, Funding acquisition, Investigation, Visualization, Writing – original draft, Writing – review & editing. MB: Data curation, Formal Analysis, Investigation, Visualization, Writing – original draft, Writing – review & editing. TD: Methodology, Writing – review & editing. AA: Methodology, Writing – review & editing. KS: Methodology, Writing – review & editing. AB: Conceptualization, Funding acquisition, Investigation, Project administration, Resources, Supervision, Writing – review & editing. MM: Conceptualization, Funding acquisition, Investigation, Project administration, Resources, Supervision, Writing – review & editing.

Funding

The author(s) declare financial support was received for the research and/or publication of this article. Research reported in this publication was supported in part by research funds to MM from Washington University School of Medicine, and by the Washington University Institute of Clinical and Translational Sciences grant #UL1TR002345 from the National Center for Advancing Translational Sciences (NCATS) of the National Institutes of Health (NIH), with Just In Time grants to BR and AB.

Conflict of interest

The authors declare that the research was conducted in the absence of any commercial or financial relationships that could be construed as a potential conflict of interest.

The author(s) declared that they were an editorial board member of Frontiers, at the time of submission. This had no impact on the peer review process and the final decision.

Generative Al statement

The author(s) declare that no Generative AI was used in the creation of this manuscript.

Any alternative text (alt text) provided alongside figures in this article has been generated by Frontiers with the support of artificial intelligence and reasonable efforts have been made to ensure accuracy, including review by the authors wherever possible. If you identify any issues, please contact us.

Publisher's note

All claims expressed in this article are solely those of the authors and do not necessarily represent those of their affiliated organizations, or those of the publisher, the editors and the reviewers. Any product that may be evaluated in this article, or claim that may be made by its manufacturer, is not guaranteed or endorsed by the publisher.

Author disclaimer

The content is solely the responsibility of the authors and does not necessarily represent the official view of the NIH.

References

- 1. World Health Organization. Number of Covid-19 Deaths Reported to Who: WHO COVID-19 dashboard(2025). Available online at: https://data.who.int/dashboards/covid19/deaths (Accessed February 1, 2025).
- 2. World Health Organization. Covid-19 Cases, World: WHO COVID-19 dashboard(2025). Available online at: https://data.who.int/dashboards/covid19/cases (Accessed February 1, 2025).
- 3. Mueller AL, McNamara MS, Sinclair DA. Why does covid-19 disproportionately affect older people? *Aging (Albany NY)*. (2020) 12:9959–81. doi: 10.18632/aging.103344
- 4. Rosenke K, Adjemian J, Munster VJ, Marzi A, Falzarano D, Onyango CO, et al. Plasmodium parasitemia associated with increased survival in ebola virus-infected patients. Clin Infect Dis. (2016) 63:1026–33. doi: 10.1093/cid/ciw452
- 5. Bartsch SM, Hotez PJ, Asti L, Zapf KM, Bottazzi ME, Diemert DJ, et al. The global economic and health burden of human hookworm infection. *PloS Negl Trop Dis.* (2016) 10:e0004922. doi: 10.1371/journal.pntd.0004922
- 6. Peng J, Federman HG, Hernandez CM, Siracusa MC. Communication is key: innate immune cells regulate host protection to helminths. *Front Immunol.* (2022) 13:995432. doi: 10.3389/fimmu.2022.995432

Supplementary material

The Supplementary Material for this article can be found online at: https://www.frontiersin.org/articles/10.3389/fimmu.2025.1701728/full#supplementary-material

SUPPLEMENTARY TABLE 1

Metadata, read mapping statistics, and SRA accessions for all RNA-seq samples.

SUPPLEMENTARY TABLE 2

Functional annotations, DEG lists, fragment counts, relative gene expression levels and DEG statistics for all genes and all DESeq comparisons.

SUPPLEMENTARY TABLE 3

DEG counts, and significantly enriched pathway counts for all DESeq comparisons.

SUPPLEMENTARY TABLE 4

FDR-adjusted P values for all significantly enriched pathways among all sets of DEGs.

SUPPLEMENTARY TABLE 5

Intersections of significantly enriched GO terms and KEGG pathways among sets of differentially expressed genes of interest. Values shown are -Log FDR-adjusted P values for enrichment among the DEG sets indicated.

SUPPLEMENTARY TABLE 6

Estimated relative abundance of 22 leukocyte cell types in each of the lung RNA-seq samples, deconvoluted using the "LM22" dataset in CIBERSORTx (with 1:1 reciprocal-best orthologs between hamster and human).

SUPPLEMENTARY FIGURE 1

Counts of significantly enriched Gene Ontology terms + KEGG pathway counts among significantly differentially expressed genes in each infected cohort relative to the uninfected controls, (A) in the lungs and (B) in the intestine. For all enrichment testing, FDR-adjusted P values \leq 0.05 were used to identify significant enrichment.

SUPPLEMENTARY FIGURE 2

Average estimated relative proportions of immune cell types, estimated by CIBERSORTx. Significance values represent two-tailed T-tests (unequal variance) compared to the Naive cohort, FDR-corrected for multiple test correction across all tests (* $P \le 0.05$, ** $P \le 0.01$, *** $P \le 0.001$). Relative proportions per sample and exact P values are provided in Supplementary Table S6. Blue shading = significantly higher, red shading = significantly lower, green shading reflects the relative abundance of each cell type in the naive sample.

- 7. Schlosser-Brandenburg J, Midha A, Mugo RM, Ndombi EM, Gachara G, Njomo D, et al. Infection with soil-transmitted helminths and their impact on coinfections. *Front Parasitol.* (2023) 2:1197956. doi: 10.3389/fpara.2023.1197956
- 8. Desai P, Karl CE, Ying B, Liang CY, Garcia-Salum T, Santana AC, et al. Intestinal helminth infection impairs vaccine-induced T cell responses and protection against Sars-Cov-2 in mice. *Sci Transl Med.* (2024) 16:eado1941. doi: 10.1126/scitranslmed.ado1941
- 9. Hartmann W, Brunn M-L, Stetter N, Gagliani N, Muscate F, Stanelle-Bertram S, et al. Helminth infections suppress the efficacy of vaccination against seasonal influenza. *Cell Rep.* (2019) 29:2243–56.e4. doi: 10.1016/j.celrep.2019.10.051
- 10. McFarlane AJ, McSorley HJ, Davidson DJ, Fitch PM, Errington C, Mackenzie KJ, et al. Enteric Helminth-Induced Type I Interferon Signaling Protects against Pulmonary Virus Infection through Interaction with the Microbiota. *J Allergy Clin Immunol.* (2017) 140:1068–78 e6. doi: 10.1016/j.jaci.2017.01.016
- 11. Desai P, Diamond MS, Thackray LB. Helminth-virus interactions: determinants of coinfection outcomes. *Gut Microbes*. (2021) 13:1961202. doi: 10.1080/19490976.2021.1961202

- 12. Wolday D, Gebrecherkos T, Arefaine ZG, Kiros YK, Gebreegzabher A, Tasew G, et al. Effect of co-infection with intestinal parasites on covid-19 severity: A prospective observational cohort study. *EClinicalMedicine*. (2021) 39:101054. doi: 10.1016/j.jeclinm.2021.101054
- 13. Al-Kuraishy HM, Al-Gareeb AI, Alkazmi L, El-Bouseary MM, Hamad RS, Abdelhamid M, et al. The potential nexus between helminths and sars-cov-2 infection: A literature review. *J Immunol Res.* (2023) 2023:5544819. doi: 10.1155/2023/5544819
- 14. Adjobimey T, Meyer J, Terkeš V, Parcina M, Hoerauf A. Helminth antigens differentially modulate the activation of Cd4(+) and Cd8(+) T lymphocytes of convalescent covid-19 patients *in vitro*. *BMC Med.* (2022) 20:241. doi: 10.1186/s12916-022-02441-x
- 15. Rissmann M, Veldhuis Kroeze EJB, Tielens AGM, Rockx B, van Hellemond JJ. Influence of a chronic schistosoma mansoni infection on the outcomes of a sars-cov-2 infection in the hamster model. *J Infect.* (2023) 87:273–6. doi: 10.1016/j.jinf.2023.07.002
- 16. Miguel DC, Brioschi MBC, Rosa LB, Minori K, Grazzia N. The impact of covid-19 on neglected parasitic diseases: what to expect? *Trends Parasitol.* (2021) 37:694–7. doi: 10.1016/j.pt.2021.05.003
- 17. Oyesola OO, Hilligan KL, Namasivayam S, Howard N, Clancy CS, Zhao M, et al. Exposure to Lung-Migrating Helminth Protects against Murine Sars-Cov-2 Infection through Macrophage-Dependent T Cell Activation. *Sci Immunol.* (2023) 8:eadf8161. doi: 10.1126/sciimmunol.adf8161
- 18. Cao Z, Wang J, Liu X, Liu Y, Li F, Liu M, et al. Helminth alleviates covid-19-related cytokine storm in an Il-9-dependent way. *mBio*. (2024) 15:e0090524. doi: 10.1128/mbio.00905-24
- 19. Scendoni R, Bury E, Lima Arrais Ribeiro I, Cingolani M, Cameriere R, De Benedictis A, et al. Leading pathogens involved in co-infection and super-infection with covid-19: forensic medicine considerations after a systematic review and meta-analysis. *Pathogens.* (2023) 12:646. doi: 10.3390/pathogens12050646
- 20. Du Y, Wang C, Zhang Y. Viral coinfections. Viruses. (2022) 14:2645. doi: 10.3390/v14122645
- 21. Dong L, Xing L. Editorial: the biological mechanism and health effect of co-infection with multiple pathogens. *Front Cell Infect Microbiol.* (2024) 14:1370067. doi: 10.3389/fcimb.2024.1370067
- 22. Bolger AM, Lohse M, Usadel B. Trimmomatic: A flexible trimmer for illumina sequence data. *Bioinformatics*. (2014) 30:2114–20. doi: 10.1093/bioinformatics/btu170
- 23. Howe KL, Achuthan P, Allen J, Allen J, Alvarez-Jarreta J, Amode MR, et al. Ensembl 2021. *Nucleic Acids Res.* (2021) 49:D884–D91. doi: 10.1093/nar/gkaa942
- 24. Dobin A, Davis CA, Schlesinger F, Drenkow J, Zaleski C, Jha S, et al. Star: ultrafast universal rna-seq aligner. *Bioinformatics*. (2013) 29:15–21. doi: 10.1093/bioinformatics/bts635
- 25. Anders S, Huber W. Differential expression analysis for sequence count data. Genome Biol. (2010) 11:R106. doi: 10.1186/gb-2010-11-10-r106
- 26. Rosa BA, Martin J, Mitreva M. R scripts for user-friendly Deseq2 rna-seq differential expression analysis. (2024). doi: 10.21203/rs.3.pex-2532/v1
- 27. Katz K, Shutov O, Lapoint R, Kimelman M, Brister JR, O'Sullivan C. The sequence read archive: A decade more of explosive growth. *Nucleic Acids Res.* (2022) 50: D387–D90. doi: 10.1093/nar/gkab1053
- 28. Kanehisa M, Furumichi M, Tanabe M, Sato Y, Morishima K. Kegg: new perspectives on genomes, pathways, diseases and drugs. *Nucleic Acids Res.* (2017) 45: D353–D61. doi: 10.1093/nar/gkw1092
- 29. Mitchell AL, Attwood TK, Babbitt PC, Blum M, Bork P, Bridge A, et al. Interpro in 2019: improving coverage, classification and access to protein sequence annotations. *Nucleic Acids Res.* (2018) 47:D351–D60. doi: 10.1093/nar/gky1100
- 30. Ge SX, Jung D, Yao R. Shinygo: A graphical gene-set enrichment tool for animals and plants. *Bioinformatics*. (2020) 36:2628–9. doi: 10.1093/bioinformatics/btz931
- 31. Gene Ontology C. The gene ontology resource: enriching a gold mine. $Nucleic\ Acids\ Res.\ (2021)\ 49:D325-D34.\ doi: 10.1093/nar/gkaa1113$
- 32. Altschul SF, Gish W, Miller W, Myers EW, Lipman DJ. Basic local alignment search tool. J Mol Biol. (1990) 215:403–10. doi: 10.1016/S0022-2836(05)80360-2
- 33. Newman AM, Steen CB, Liu CL, Gentles AJ, Chaudhuri AA, Scherer F, et al. Determining cell type abundance and expression from bulk tissues with digital cytometry. *Nat Biotechnol.* (2019) 37:773–82. doi: 10.1038/s41587-019-0114-2
- 34. Newman AM, Liu CL, Green MR, Gentles AJ, Feng W, Xu Y, et al. Robust enumeration of cell subsets from tissue expression profiles. *Nat Methods.* (2015) 12:453–7. doi: 10.1038/nmeth.3337
- 35. Imai M, Iwatsuki-Horimoto K, Hatta M, Loeber S, Halfmann PJ, Nakajima N, et al. Syrian hamsters as a small animal model for Sars-Cov-2 infection and countermeasure development. *Proc Natl Acad Sci U.S.A.* (2020) 117:16587–95. doi: 10.1073/pnas.2009799117
- 36. Shou S, Liu M, Yang Y, Kang N, Song Y, Tan D, et al. Animal models for covid-19: hamsters, mouse, ferret, mink, tree shrew, and non-human primates. *Front Microbiol.* (2021) 12:626553. doi: 10.3389/fmicb.2021.626553
- 37. McMahan K, Giffin V, Tostanoski LH, Chung B, Siamatu M, Suthar MS, et al. Reduced pathogenicity of the Sars-Cov-2 omicron variant in hamsters. *Med.* (2022) 3:262–8 e4. doi: 10.1016/j.medj.2022.03.004

- 38. Francis ME, Goncin U, Kroeker A, Swan C, Ralph R, Lu Y, et al. Sars-Cov-2 infection in the Syrian hamster model causes inflammation as well as type I interferon dysregulation in both respiratory and non-respiratory tissues including the heart and kidney. *PloS Pathog.* (2021) 17:e1009705. doi: 10.1371/journal.ppat.1009705
- 39. Chan JF, Zhang AJ, Yuan S, Poon VK, Chan CC, Lee AC, et al. Simulation of the clinical and pathological manifestations of coronavirus disease 2019 (Covid-19) in a golden Syrian hamster model: implications for disease pathogenesis and transmissibility. *Clin Infect Dis.* (2020) 71:2428–46. doi: 10.1093/cid/ciaa325
- 40. Bagato O, Balkema-Buschmann A, Todt D, Weber S, Gomer A, Qu B, et al. Spatiotemporal analysis of Sars-Cov-2 infection reveals an expansive wave of monocyte-derived macrophages associated with vascular damage and virus clearance in hamster lungs. *Microbiol Spectr.* (2024) 12:e0246923. doi: 10.1128/spectrum.02469-23
- 41. Zhang J, Xu E, Ren C, Yan W, Zhang M, Chen M, et al. Mice deficient in Rbm38, a target of the P53 family, are susceptible to accelerated aging and spontaneous tumors. *Proc Natl Acad Sci U.S.A.* (2014) 111:18637–42. doi: 10.1073/pnas.1415607112
- 42. Yao Y, Sun H, Chen Y, Tian L, Huang D, Liu C, et al. Rbm24 inhibits the translation of Sars-Cov-2 polyproteins by targeting the 5'-untranslated region. *Antiviral Res.* (2023) 209:105478. doi: 10.1016/j.antiviral.2022.105478
- 43. Juliana CA, Yang J, Rozo AV, Good A, Groff DN, Wang SZ, et al. Atf5 regulates beta-cell survival during stress. *Proc Natl Acad Sci U.S.A.* (2017) 114:1341–6. doi: 10.1073/pnas.1620705114
- 44. Sears TK, Angelastro JM. The transcription factor atf5: role in cellular differentiation, stress responses, and cancer. *Oncotarget*. (2017) 8:84595–609. doi: 10.18632/oncotarget.21102
- 45. Gasser R, Cloutier M, Prevost J, Fink C, Ducas E, Ding S, et al. Major role of Igm in the neutralizing activity of convalescent plasma against Sars-Cov-2. *Cell Rep.* (2021) 34:108790. doi: 10.1016/j.celrep.2021.108790
- 46. Sadowska-Bartosz I, Bartosz G. Peroxiredoxin 2: an important element of the antioxidant defense of the erythrocyte. *Antioxid (Basel)*. (2023) 12:1012. doi: 10.3390/antiox12051012
- 47. Castro CD, Flajnik MF. Putting J chain back on the map: how might its expression define plasma cell development? *J Immunol.* (2014) 193:3248–55. doi: 10.4049/jimmunol.1400531
- 48. Kawasaki K, Ohta Y, Castro CD, Flajnik MF. The immunoglobulin J chain is an evolutionarily co-opted chemokine. *Proc Natl Acad Sci.* (2024) 121:e2318995121. doi: 10.1073/pnas.2318995121
- 49. Esmat K, Jamil B, Kheder RK, Kombe Kombe AJ, Zeng W, Ma H, et al. Immunoglobulin a response to Sars-Cov-2 infection and immunity. *Heliyon*. (2024) 10:e24031. doi: 10.1016/j.heliyon.2024.e24031
- 50. Branco ACCC, Rogers LM, Aronoff DM. Folate receptor beta signaling in the regulation of macrophage antimicrobial immune response: A scoping review. *Biomed Hub.* (2024) 9:31–7. doi: 10.1159/000536186
- 51. Ma J, Zhen X, Huang X, Jiang X. Folic acid supplementation repressed hypoxia-induced inflammatory response via ros and Jak2/Stat3 pathway in human promyelomonocytic cells. *Nutr Res.* (2018) 53:40–50. doi: 10.1016/j.nutres.2018.03.007
- 52. Samblas M, Martínez JA, Milagro F. Folic acid improves the inflammatory response in lps-activated thp-1 macrophages. *Mediators Inflammation*. (2018) 2018:1312626. doi: 10.1155/2018/1312626
- 53. Moon SH, Liu X, Cedars AM, Yang K, Kiebish MA, Joseph SM, et al. Heart failure-induced activation of phospholipase Ipla(2)Gamma generates hydroxyeicosatetraenoic acids opening the mitochondrial permeability transition pore. *J Biol Chem.* (2018) 293:115–29. doi: 10.1074/jbc.RA117.000405
- 54. Ghosh M, Loper R, Ghomashchi F, Tucker DE, Bonventre JV, Gelb MH, et al. Function, activity, and membrane targeting of cytosolic phospholipase a(2)Zeta in mouse lung fibroblasts. *J Biol Chem.* (2007) 282:11676–86. doi: 10.1074/jbc.M608458200
- 55. Chalkidi N, Paraskeva C, Koliaraki V. Fibroblasts in intestinal homeostasis, damage, and repair. *Front Immunol.* (2022) 13:924866. doi: 10.3389/fimmu.2022.924866
- 56. Kikut J, Mokrzycka M, Drozd A, Grzybowska-Chlebowczyk U, Zietek M, Szczuko M. Involvement of proinflammatory arachidonic acid (Ara) derivatives in Crohn's disease (Cd) and ulcerative colitis (Uc). *J Clin Med.* (2022) 11:1861. doi: 10.3390/jcm11071861
- 57. Entwistle LJ, Pelly VS, Coomes SM, Kannan Y, Perez-Lloret J, Czieso S, et al. Epithelial-cell-derived phospholipase a(2) group 1b is an endogenous anthelmintic. *Cell Host Microbe*. (2017) 22:484–93.e5. doi: 10.1016/j.chom.2017.09.006
- 58. Nguyen HC, Bu S, Nikfarjam S, Rasheed B, Michels DCR, Singh A, et al. Loss of fatty acid binding protein 3 ameliorates lipopolysaccharide-induced inflammation and endothelial dysfunction. *J Biol Chem.* (2023) 299:102921. doi: 10.1016/j.jbc.2023.102921
- 59. Assante G, Tourna A, Carpani R, Ferrari F, Prati D, Peyvandi F, et al. Reduced circulating Fabp2 in patients with moderate to severe Covid-19 may indicate enterocyte functional change rather than cell death. *Sci Rep.* (2022) 12:18792. doi: 10.1038/s41598-022-23282-x
- 60. Court MH, Hazarika S, Krishnaswamy S, Finel M, Williams JA. Novel polymorphic human udp-glucuronosyltransferase 2a3: cloning, functional

characterization of enzyme variants, comparative tissue expression, and gene induction. *Mol Pharmacol.* (2008) 74:744–54. doi: 10.1124/mol.108.045500

- 61. Li J, Chen Y, Li R, Zhang X, Chen T, Mei F, et al. Gut microbial metabolite hyodeoxycholic acid targets the Tlr4/Md2 complex to attenuate inflammation and protect against sepsis. *Mol Ther.* (2023) 31:1017–32. doi: 10.1016/j.ymthe.2023.01.018
- $62.\,$ Markovich D. Na+-sulfate cotransporter Slc13a1. Pflugers Arch. (2014) 466:131–7. doi: 10.1007/s00424-013-1388-8
- 63. Dawson PA, Huxley S, Gardiner B, Tran T, McAuley JL, Grimmond S, et al. Reduced mucin sulfonation and impaired intestinal barrier function in the hyposulfataemic nas1 null mouse. *Gut.* (2009) 58:910–9. doi: 10.1136/gut.2007.147595
- 64. Szafran BN, Borazjani A, Scheaffer HL, Crow JA, McBride AM, Adekanye O, et al. Carboxylesterase 1d inactivation augments lung inflammation in mice. ACS Pharmacol Transl Sci. (2022) 5:919–31. doi: 10.1021/acsptsci.2c00098
- 65. Lian J, Nelson R, Lehner R. Carboxylesterases in lipid metabolism: from mouse to human. *Protein Cell.* (2018) 9:178–95. doi: 10.1007/s13238-017-0437-z
- 66. Yan D, Ye S, He Y, Wang S, Xiao Y, Xiang X, et al. Fatty acids and lipid mediators in inflammatory bowel disease: from mechanism to treatment. *Front Immunol.* (2023) 14:1286667. doi: 10.3389/fimmu.2023.1286667
- 67. Lejeune J, Brachet G, Watier H. Evolutionary story of the low/medium-affinity Igg fc receptor gene cluster. *Front Immunol.* (2019) 10:1297. doi: 10.3389/fimmu.2019.01297
- 68. Junqueira C, Crespo A, Ranjbar S, de Lacerda LB, Lewandrowski M, Ingber J, et al. Fcgammar-mediated Sars-Cov-2 infection of monocytes activates inflammation. *Nature*. (2022) 606:576–84. doi: 10.1038/s41586-022-04702-4
- 69. Fujiwara RT, Cancado GG, Freitas PA, Santiago HC, Massara CL, Dos Santos Carvalho O, et al. Necator americanus infection: A possible cause of altered dendritic cell differentiation and eosinophil profile in chronically infected individuals. *PloS Negl Trop Dis.* (2009) 3:e399. doi: 10.1371/journal.pntd.0000399
- 70. Missailidis D, Ebrahimie E, Dehcheshmeh MM, Allan C, Sanislav O, Fisher P, et al. A blood-based mrna signature distinguishes people with long covid from recovered individuals. *Front Immunol*. (2024) 15:1450853. doi: 10.3389/fimmu.2024.1450853
- 71. Bollavaram K, Leeman TH, Lee MW, Kulkarni A, Upshaw SG, Yang J, et al. Multiple sites on Sars-Cov-2 spike protein are susceptible to proteolysis by cathepsins B, K, L, S and V. *Protein Sci.* (2021) 30:1131–43. doi: 10.1002/pro.4073
- 72. Srivastava M, Steinwede K, Kiviranta R, Morko J, Hoymann HG, Langer F, et al. Overexpression of cathepsin K in mice decreases collagen deposition and lung resistance in response to bleomycin-induced pulmonary fibrosis. *Respir Res.* (2008) 9:54. doi: 10.1186/1465-9921-9-54
- 73. Arampatzidou M, Schütte A, Hansson GC, Saftig P, Brix K. Effects of cathepsin K deficiency on intercellular junction proteins, luminal mucus layers, and extracellular matrix constituents in the mouse colon. *Biol Chem.* (2012) 393:1391–403. doi: 10.1515/hsz-2012-0204
- 74. De Lorenzo R, Sciorati C, Lore NI, Capobianco A, Tresoldi C, Cirillo DM, et al. Chitinase-3-like protein-1 at hospital admission predicts covid-19 outcome: A prospective cohort study. *Sci Rep.* (2022) 12:7606. doi: 10.1038/s41598-022-11532-x
- 75. Kamle S, Ma B, Lee CM, Schor G, Zhou Y, Lee CG, et al. Host chitinase 3-like-1 is a universal therapeutic target for Sars-Cov-2 viral variants in Covid-19. *Elife.* (2022) 11:e78273. doi: 10.7554/eLife.78273
- 76. Curtiss ML, Rosenberg AF, Scharer CD, Mousseau B, Benavides NAB, Bradley JE, et al. Chitinase-3-like 1 regulates T(H)2 cells, T(Fh) cells and ige responses to helminth infection. *Front Immunol.* (2023) 14:1158493. doi: 10.3389/fimmu.2023.1158493
- 77. Mizoguchi E. Chitinase 3-like-1 exacerbates intestinal inflammation by enhancing bacterial adhesion and invasion in colonic epithelial cells. *Gastroenterology*. (2006) 130:398-411. doi: 10.1053/j.gastro.2005.12.007
- 78. Loukas A, Hotez PJ, Diemert D, Yazdanbakhsh M, McCarthy JS, Correa-Oliveira R, et al. Hookworm infection. *Nat Rev Dis Primers*. (2016) 2:16088. doi: 10.1038/nrdp.2016.88
- 79. Mantovani S, Oliviero B, Varchetta S, Renieri A, Mondelli MU. Tlrs: innate immune sentries against Sars-Cov-2 infection. *Int J Mol Sci.* (2023) 24:8065. doi: 10.3390/ijms24098065
- 80. Ryter SW. Heme oxygenase-1: an anti-inflammatory effector in cardiovascular, lung, and related metabolic disorders. *Antioxid (Basel)*. (2022) 11:555. doi: 10.3390/antiox11030555
- 81. Hara Y, Tsukiji J, Yabe A, Onishi Y, Hirose H, Yamamoto M, et al. Heme oxygenase-1 as an important predictor of the severity of Covid-19. *PloS One.* (2022) 17: e0273500. doi: 10.1371/journal.pone.0273500
- 82. Batra N, De Souza C, Batra J, Raetz AG, Yu AM. The hmox1 pathway as a promising target for the treatment and prevention of Sars-Cov-2 of 2019 (Covid-19). *Int J Mol Sci.* (2020) 21:6412. doi: 10.3390/ijms21176412
- 83. Lujan RA, Pei L, Shannon JP, Dábilla N, Dolan PT, Hickman HD. Widespread and dynamic expression of granzyme C by skin-resident antiviral T cells. *Front Immunol.* (2023) 14:1236595. doi: 10.3389/fimmu.2023.1236595
- 84. de Jong LC, Crnko S, Ten Broeke T, Bovenschen N. Noncytotoxic functions of killer cell granzymes in viral infections. *PloS Pathog.* (2021) 17:e1009818. doi: 10.1371/journal.ppat.1009818

- 85. Nagozir S, Shakouri Khomartash M, Parsania M, Vahidi M, Ghorbani M. Association between genetic variants in the Cd209 gene and susceptibility to covid-19 in Iranian population. *Hum Gene*. (2023) 38:201215. doi: 10.1016/j.humgen.2023.201215
- 86. Ficial M, Antonaglia C, Chilosi M, Santagiuliana M, Tahseen AO, Confalonieri D, et al. Keratin-14 expression in pneumocytes as a marker of lung regeneration/repair during diffuse alveolar damage. *Am J Respir Crit Care Med.* (2014) 189:1142–5. doi: 10.1164/rccm.201312-2134LE
- 87. Chang CY, Huang YC, Chiang HH, Wu YY, Wu KL, Chang YY, et al. Ladinin 1 shortens survival via promoting proliferation and enhancing invasiveness in lung adenocarcinoma. *Int J Mol Sci.* (2022) 24:431. doi: 10.3390/ijms24010431
- 88. Synolaki E, Papadopoulos V, Divolis G, Tsahouridou O, Gavriilidis E, Loli G, et al. The activin/follistatin axis is severely deregulated in Covid-19 and independently associated with in-hospital mortality. *J Infect Dis.* (2021) 223:1544–54. doi: 10.1093/infdis/iiab108
- 89. Group P-CC. Clinical characteristics with inflammation profiling of long covid and association with 1-year recovery following hospitalisation in the UK: A prospective observational study. *Lancet Respir Med.* (2022) 10:761–75. doi: 10.1016/S2213-2600 (22)00127-8
- 90. Warren DS, Morrell JC, Moser HW, Valle D, Gould SJ. Identification of Pex10, the gene defective in complementation group 7 of the peroxisome-biogenesis disorders. *Am J Hum Genet.* (1998) 63:347–59. doi: 10.1086/301963
- 91. Kronstein-Wiedemann R, Stadtmuller M, Traikov S, Georgi M, Teichert M, Yosef H, et al. Sars-Cov-2 infects red blood cell progenitors and dysregulates hemoglobin and iron metabolism. *Stem Cell Rev Rep.* (2022) 18:1809–21. doi: 10.1007/s12015-021-10322-8
- 92. Byrne A, Manalo G, Clarke NE, Vaz Nery S. Impact of hookworm infection and preventive chemotherapy on haemoglobin in non-pregnant populations. *Trop Med Int Health.* (2021) 26:1568–92. doi: 10.1111/tmi.13681
- 93. Tong M, Jiang Y, Xia D, Xiong Y, Zheng Q, Chen F, et al. Elevated expression of serum endothelial cell adhesion molecules in Covid-19 patients. *J Infect Dis.* (2020) 222:894–8. doi: 10.1093/infdis/iiaa349
- 94. Wu S, Xu Y, Zhang J, Ran X, Jia X, Wang J, et al. Longitudinal serum proteome characterization of covid-19 patients with different severities revealed potential therapeutic strategies. *Front Immunol*. (2022) 13:893943. doi: 10.3389/fimmu.2022.893943
- 95. Zhu R, Chen Y-T, Wang B-W, You Y-Y, Wang X-H, Xie H-T, et al. Tap1, a potential immune-related prognosis biomarker with functional significance in uveal melanoma. *BMC Cancer*. (2023) 23:146. doi: 10.1186/s12885-023-10527-9
- 96. Ning S, Pagano JS, Barber GN. Irf7: activation, regulation, modification and function. *Genes Immun*. (2011) 12:399–414. doi: 10.1038/gene.2011.21
- 97. Zhang Y, Wang J, Yu C, Xia K, Yang B, Zhang Y, et al. Advances in single-cell sequencing and its application to musculoskeletal system research. *Cell Prolif.* (2022) 55:e13161. doi: 10.1111/cpr.13161
- 98. Betancor G. You shall not pass: Mx2 proteins are versatile viral inhibitors. *Vaccines (Basel)*. (2023) 11:930. doi: 10.3390/vaccines11050930
- 99. Bizzotto J, Sanchis P, Abbate M, Lage-Vickers S, Lavignolle R, Toro A, et al. Sars-Cov-2 infection boosts mx1 antiviral effector in covid-19 patients. *iScience*. (2020) 23:101585. doi: 10.1016/j.isci.2020.101585
- 100. Harioudh MK, Perez J, Chong Z, Nair S, So L, McCormick KD, et al. Oligoadenylate synthetase 1 displays dual antiviral mechanisms in driving translational shutdown and protecting interferon production. *Immunity.* (2024) 57:446–61 e7. doi: 10.1016/j.immuni.2024.02.002
- 101. Jain S, Rego S, Park S, Liu Y, Parn S, Savsani K, et al. Rnaseq profiling of covid19-infected patients identified an Eif2ak2 inhibitor as a potent Sars-Cov-2 antiviral. *Clin Transl Med.* (2022) 12:e1098. doi: 10.1002/ctm2.1098
- 102. Tolomeo M, Cavalli A, Cascio A. Stat1 and its crucial role in the control of viral infections. *Int J Mol Sci.* (2022) 23:4095. doi: 10.3390/ijms23084095
- 103. Huang M, Mark A, Pham J, Vera K, Saravia-Butler AM, Beheshti A, et al. Rna editing regulates host immune response and T cell homeostasis in Sars-Cov-2 infection. *PloS One.* (2024) 19:e0307450. doi: 10.1371/journal.pone.0307450
- 104. Boudewijns R, Thibaut HJ, Kaptein SJF, Li R, Vergote V, Seldeslachts L, et al. Stat2 signaling restricts viral dissemination but drives severe pneumonia in Sars-Cov-2 infected hamsters. *Nat Commun.* (2020) 11:5838. doi: 10.1038/s41467-020-19684-y
- 105. Zhao YC, Wang TJ, Cui J, She LZ, Zhang RF, Zhang CH. The role of Slc39a4 in the prognosis, immune microenvironment, and contribution to Malignant behavior *in vivo* and *in vitro* of cervical cancer. *Transl Oncol.* (2024) 40:101839. doi: 10.1016/j.tranon.2023.101839
- 106. Smith JL, Brooker S. Impact of hookworm infection and deworming on anaemia in non-pregnant populations: A systematic review. *Trop Med Int Health.* (2010) 15:776–95. doi: 10.1111/j.1365-3156.2010.02542.x
- 107. Dunaway LS, Loeb SA, Petrillo S, Tolosano E, Isakson BE. Heme metabolism in nonerythroid cells. *J Biol Chem.* (2024) 300:107132. doi: 10.1016/j.jbc.2024.107132
- 108. Kaneko K, Furuyama K, Fujiwara T, Kobayashi R, Ishida H, Harigae H, et al. Identification of a novel erythroid-specific enhancer for the alas2 gene and its loss-of-function mutation which is associated with congenital sideroblastic anemia. *Haematologica*. (2014) 99:252–61. doi: 10.3324/haematol.2013.085449

- 109. Kant TA, Newe M, Winter L, Hoffmann M, Kammerer S, Klapproth E, et al. Genetic deletion of polo-like kinase 2 induces a pro-fibrotic pulmonary phenotype. *Cells.* (2021) 10:617. doi: 10.3390/cells10030617
- 110. Di Vito C, Calcaterra F, Coianiz N, Terzoli S, Voza A, Mikulak J, et al. Natural killer cells in Sars-Cov-2 infection: pathophysiology and therapeutic implications. *Front Immunol.* (2022) 13:888248. doi: 10.3389/fimmu.2022.888248
- 111. Park YJ, Acosta D, Rubel Hoq M, Khurana S, Golding H, Zaitseva M. Pyrogenic and inflammatory mediators are produced by polarized M1 and M2 macrophages activated with D-dimer and Sars-Cov-2 spike immune complexes. *Cytokine*. (2024) 173:156447. doi: 10.1016/j.cyto.2023.156447
- 112. Meneses-Preza YG, Soria-Castro R, Alfaro-Doblado AR, Hernandez-Solis A, Alvarez-Maldonado P, Gomez-Martin D, et al. Mast cell activation signature as a potential biomarker in Covid-19. *Immunol Lett.* (2025) 275:107026. doi: 10.1016/j.imlet 2025 107026
- 113. Nair MG, Herbert DR. Immune polarization by hookworms: taking cues from T helper type 2, type 2 innate lymphoid cells and alternatively activated macrophages. *Immunology.* (2016) 148:115–24. doi: 10.1111/imm.12601
- 114. Periago MV, Bethony JM. Hookworm virulence factors: making the most of the host. *Microbes Infect*. (2012) 14:1451-64. doi: 10.1016/j.micinf.2012.09.002